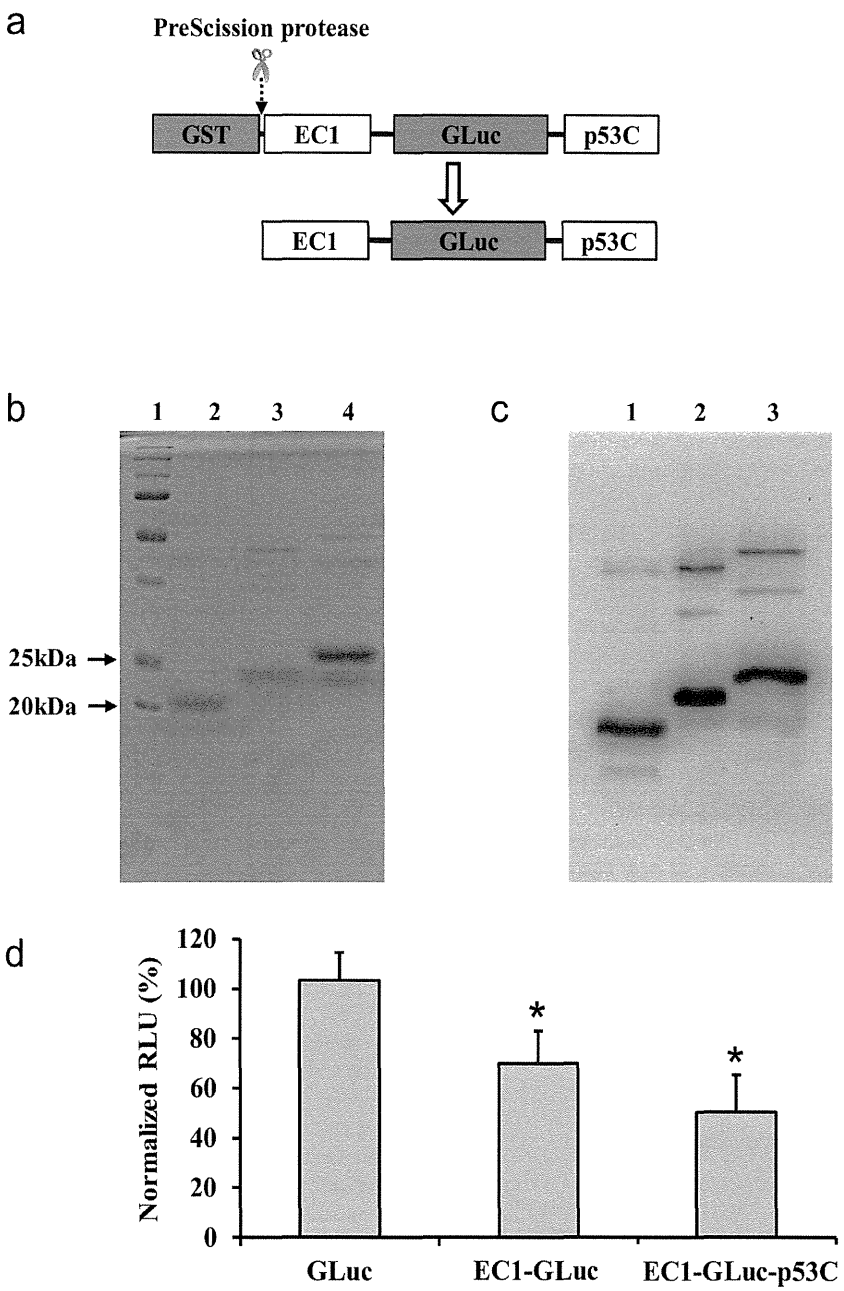

Fig.1. Han et al

Figure 1. Purification and activity of the recombinant proteins. a) Schema of the purification of EC1-GLuc-p53C with the GST expression system. The GST tag was cleaved by PreScission protease after purification. b) Coomassie brilliant blue staining of purified proteins after 15% SDS-PAGE. Lane 1~4 are marker, GLuc, EC1-GLuc and EC1-GLuc-p53C, respectively. c) The purified proteins after 15% SDS-PAGE were detected using Western blotting with rabbit anti-*Gaussia* Luciferase serum. Lanes 1~3 are GLuc, EC1-GLuc and EC1-GLuc-p53C, respectively. d) Bioluminescent activities of the purified proteins. Each protein (2 μg) was evaluated using a plate luminometer. The bioluminescent values of EC1-GLuc and EC1-GLuc-p53C were normalized with GLuc. n=6 each, * $p<0.01$.

doi: 10.1371/journal.pone.0075288.g001

The stability of GLuc, EC1-GLuc and EC1-GLuc-p53C was evaluated by incubation in mouse serum at 37°C. The stability of GLuc was improved by the fusion of EC1 and p53C. The half-life of the luminescent activity of GLuc was determined as 18.6 hours, while that of EC1-GLuc and EC1-GLuc-p53C was 189.5 and 216 hours, respectively (Figure 2a). As a result, the bioluminescent activity of EC1-GLuc-p53C reached 92% that of GLuc at 3 h after incubation in serum (Figure 2b). In addition, the degradation of the three proteins in serum was also examined by Western blotting using anti-GLuc antibody. All three proteins were stable against degradation when incubated in serum at 37°C (Figure 2c). These results suggest the bioluminescent activity and stability of EC1-GLuc-p53C to be suitable for application both *in vitro* and *in vivo*.

EC1-GLuc-p53C targets ErbB2 for bioluminescence imaging *in vitro*

Two human breast carcinoma cell lines, MCF7 and BT474, were used to evaluate the ErbB2-targeted imaging *in vitro*. The overexpression of ErbB2 in BT474 was confirmed by Western blotting, while the expression of ErbB2 in MCF7 cells was undetectable (Figure 3a). To detect the ErbB2-targeted bioluminescence, MCF7 and BT474 cells were treated with 1 μM of the recombinant proteins. A strong signal was detected in ErbB2-overexpressing BT474 cells incubated with EC1-GLuc and EC1-GLuc-p53C (Figure 3b, Figure S1). In contrast, no significant bioluminescence was observed in MCF7 cells incubated with each protein (Figure 3b, Figure S1). Moreover, internalization of the recombinant proteins was also observed in BT474 cells incubated with EC1-GLuc and EC1-GLuc-p53C, and the internalization of EC1-fused proteins was mostly undetectable, when the extra-cellular domain of ErbB2 was blocked by anti-ErbB2 antibody (Figure 3c). These results suggest that EC1-GLuc and EC1-GLuc-p53C retain affinity for ErbB2, and are internalized in ErbB2-overexpressing cells *in vitro*.

EC1-GLuc-p53C selectively inhibits proliferation of ErbB2-overexpressing BT474 Cells

WST-1 assay was used to evaluate effect of the recombinant proteins on the proliferation of MCF7 and BT474 cells. EC1-GLuc-p53C significantly inhibited the proliferation of BT474 but not MCF7 cells on day 3 and 4 (Figure 4a). The control proteins, GLuc and EC1-GLuc, had no significant effect on the proliferation of either cell line (Figure 4a). Moreover, effect of EC1-GLuc-p53C on the proliferation of BT474 was dose-dependent (Figure 4b). In addition, the results of luciferase reporter Assay for p53-driven Transactivation indicated that p53C peptide was active and reactivated endogenous p53 when internalized in BT474 cells (Figure 4c). Taken together, these results suggest that the inhibitory effect of EC1-GLuc-p53C on proliferation of cancer cells has an ErbB2-targeting property and is due to the efficacy of p53C peptide in the fusion protein.

EC1-GLuc-p53C targets ErbB2 for bioluminescence imaging *in vivo*

For the experiments *in vivo*, we prepared mice with MCF7 and BT474 xenografted tumors on both flanks. Histological observations of the tumors were made using H&E staining (Figure S2a). High expression of ErbB2 in BT474 tumors was also confirmed by IF staining (Figure S2b). To evaluate the ErbB2-targeting property of EC1-GLuc-p53C *in vivo*, the retention of EC1-GLuc-p53C in tumors after intratumoral injection was examined by IF staining with anti-GLuc antibody. EC1-GLuc-p53C was detectable in BT474 tumors for up to 24 h after the injection. In contrast, EC1-GLuc-p53C was only weakly detected in MCF7 tumors up to 6 h after the injection (Figure 5). The result suggests the retention time of EC1-GLuc-p53C to be much longer in BT474 than MCF7 tumors. Based on the retention time of EC1-GLuc-p53C in tumors, bioluminescent images were acquired 6, 8, 12 and 24 h after the protein injection. Signal was detected in BT474 tumors for up to 24 h, while it was undetectable at MCF7 tumor sites 8 h after the protein injection (Figure 6). These results suggest that the ErbB2-targeting property of EC1-GLuc-p53C facilitates its retention in BT474 tumors and bioluminescence imaging *in vivo*.

ErbB2-targeted tumor growth inhibition by EC1-GLuc-p53C

To examine the effect of EC1-GLuc-p53C on tumor growth, mice bearing MCF7 and BT474 tumors with an average volume of ~110mm^3±10mm^3 were intratumorally injected with 15 μg of protein every day for 5 days. After treatment, all mice were monitored by measuring tumor volume. The data are plotted in Figure 7. EC1-GLuc-p53C inhibited the growth of BT474 tumors from day 9 after treatment. In contrast, no significant therapeutic effect of the protein was observed in MCF7 tumors. These results suggest that the inhibitory effect of EC1-GLuc-p53C on tumor growth involves the targeting of ErbB2. To clarify the therapeutic effect of EC1-GLuc-p53C on BT474 tumor is due to the efficacy of p53C peptide, BT474 tumors further received treatment with 30 μL of GLuc, EC1-GLuc, EC1-GLuc-p53C (0.5 μg/μL) or the same volume of PBS. Results showed that only EC1-GLuc-p53C significantly inhibited the growth of BT474 tumors (Figure S3). It indicates that the inhibitory effect of EC1-GLuc-p53C on the tumor growth has an ErbB2-targeting property and is derived from the efficacy of p53C peptide in the fusion protein, which is similar to those *in vitro*.

Discussion

With advances in cancer biology, some surface molecules specifically overexpressed in cancer cells have been identified. Among them, the ErbB/EGFR family is one of the best known. In addition, progress in molecular biology has provided new techniques for developing biomolecules to target molecules of interest for cancer diagnosis and therapy [17]. Previously, we developed an immunoliposome conjugated with anti-EGFR antibody, which successfully targeted glioma cells for delivery of BSH and bioluminescence imaging *in vitro* and *in vivo*

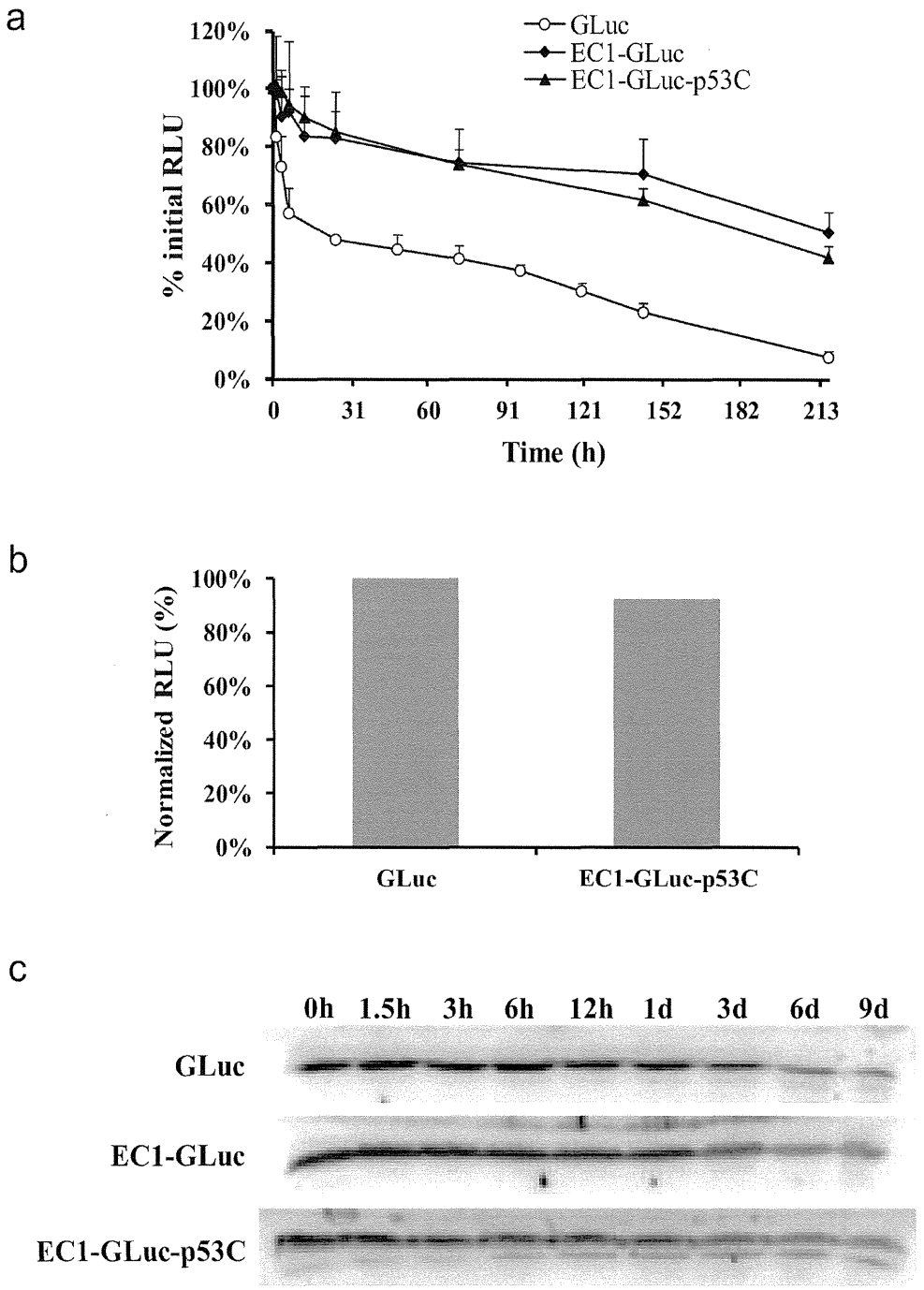

Fig.2. Han et al

Figure 2. Stability and bioluminescent activity of the recombinant proteins in serum. Proteins incubated with an equal volume of mouse serum at 37°C were withdrawn at the indicated time points for bioluminescent activity evaluation (a) and Western blotting (c). b) The bioluminescent activity of EC1-GLuc-p53C and GLuc was examined 3 h after incubation in serum. The bioluminescent values of EC1-GLuc-p53C were normalized with GLuc. n = 6 each.

doi: 10.1371/journal.pone.0075288.g002

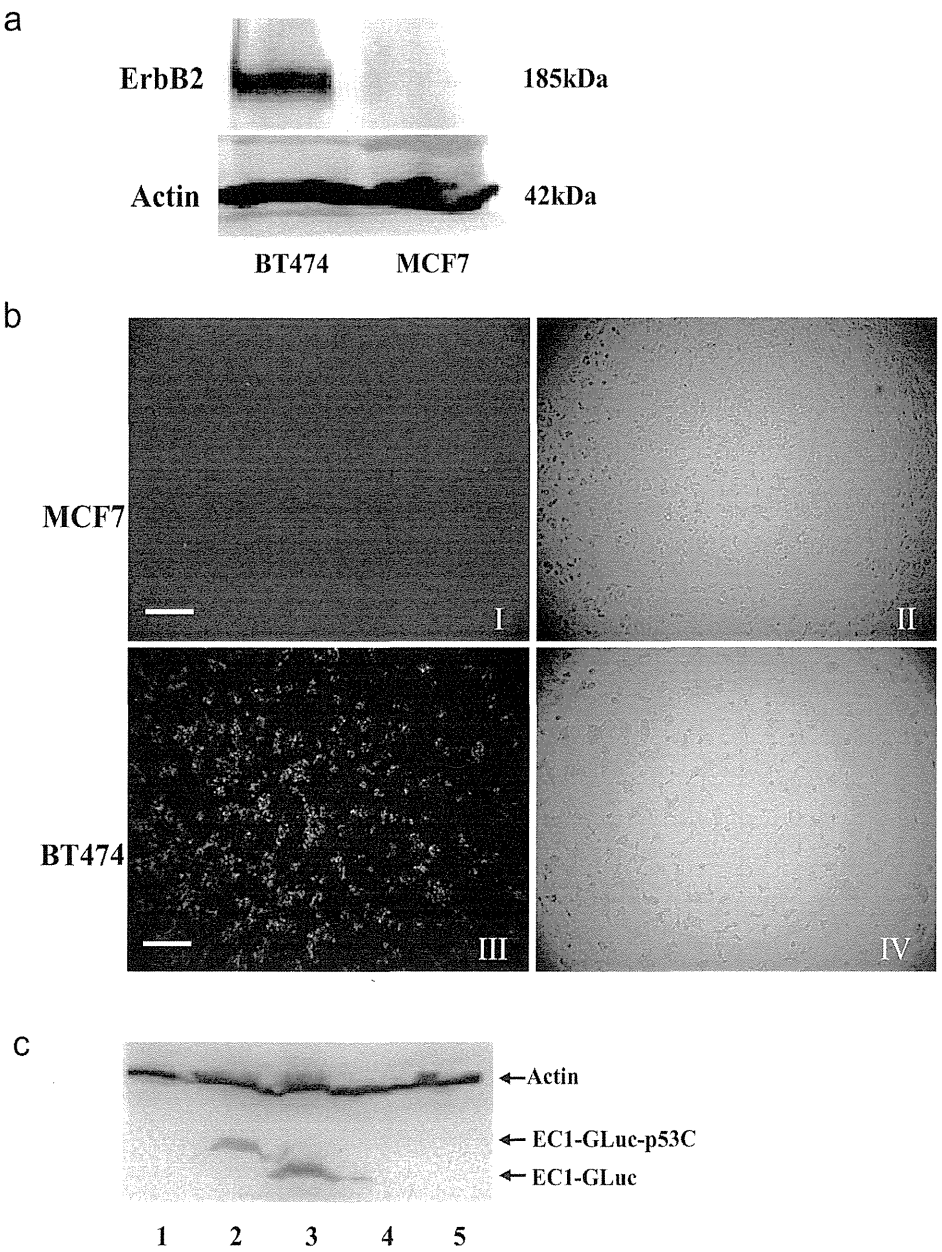

Fig.3. Han et al

Figure 3. ErbB2-targeted bioluminescence imaging of EC1-GLuc-p53C *in vitro*. a) Expression of ErbB2 in MCF7 and BT474 cells. Cell lysate of the two cell lines was subjected to 6% SDS-PAGE and immunoblotted with anti-ErbB2 antibody. β-actin was used as an endogenous control. b) Bioluminescence imaging *in vitro*. Cells incubated with 1 μM of EC-GLuc-p53C were washed with culture medium without serum. Images were acquired with a bioluminescence microscope immediately after the addition of 1 μg/mL CTZ. I and III, bioluminescence images; II and IV, phase-contrast images. Bar = 100 μm. c) Internalization of EC1-fused proteins into ErbB2-overexpressing BT474 cells. Cells were incubated with 1 μM of protein for 24 h, lane 1: GLuc; lane 2: EC-GLuc-p53C; lane 3: EC-GLuc; lane 4: anti-ErbB2+EC1-GLuc-p53C; lane 5: anti-ErbB2+EC-GLuc. The internalization of fusion protein was immunoblotted with rabbit anti-*Gaussia* Luciferase serum. β-actin was used as an endogenous control.

doi: 10.1371/journal.pone.0075288.g003

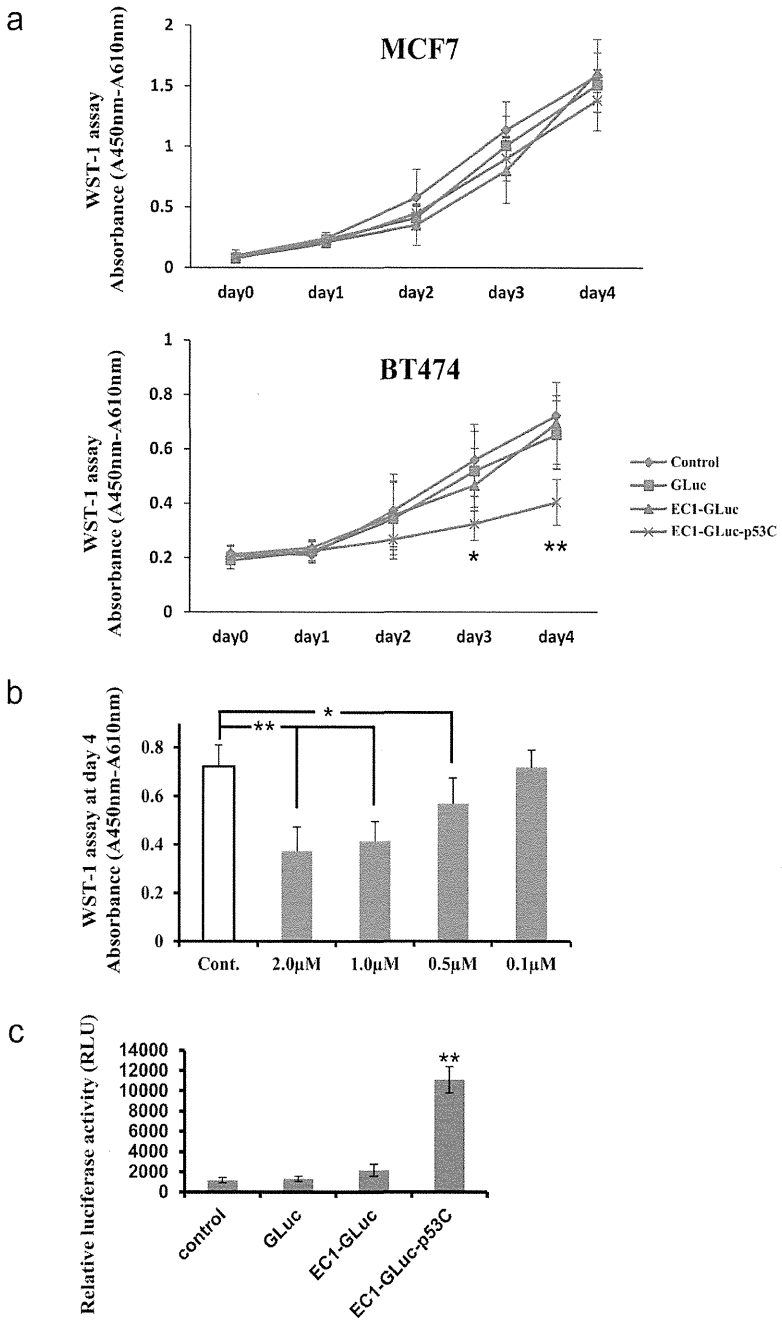

Fig.4. Han et al

Figure 4. Effect of EC1-GLuc-p53C on proliferation of MCF7 and BT474 cells. a) Time-dependent changes in proliferation of MCF7 (top panel) and BT474 (bottom panel) cells. Cells were supplemented with 1 μM of each recombinant protein or PBS (control) on day 0 and further cultured 96 h (day 4). Cellular proliferation was assessed by the WST-1 assay every 24 h. ♦, PBS (control); ■, GLuc; ▲, EC1-GLuc; ×, EC1-GLuc-p53C. n = 6 each. *p<0.05 and **p<0.01 vs control. b) Dose-dependent effect of EC1-GLuc-p53C on the proliferation of BT474 cells. BT474 cells were treated with EC1-GLuc-p53C at various concentrations or PBS (Cont.), and WST-1 assay was performed on day 4. n = 6 each. *, $p < 0.05$; **, $p < 0.01$. c) p53-driven transcriptional activity with the $p21^{WAF1}$ luciferace reporter assay. BT474 transfected with the luciferase reporter vector were incubated with 1μM of GLuc, EC1-GLuc, EC1-GLuc-p53C or PBS for 24h. $p21^{WAF1}$ luciferase reporter activities in cells were measured with Luciferase Assay System. Data are presented as the mean±S.E.M. *n* = 5 in each group; **P < 0.01.

doi: 10.1371/journal.pone.0075288.g004

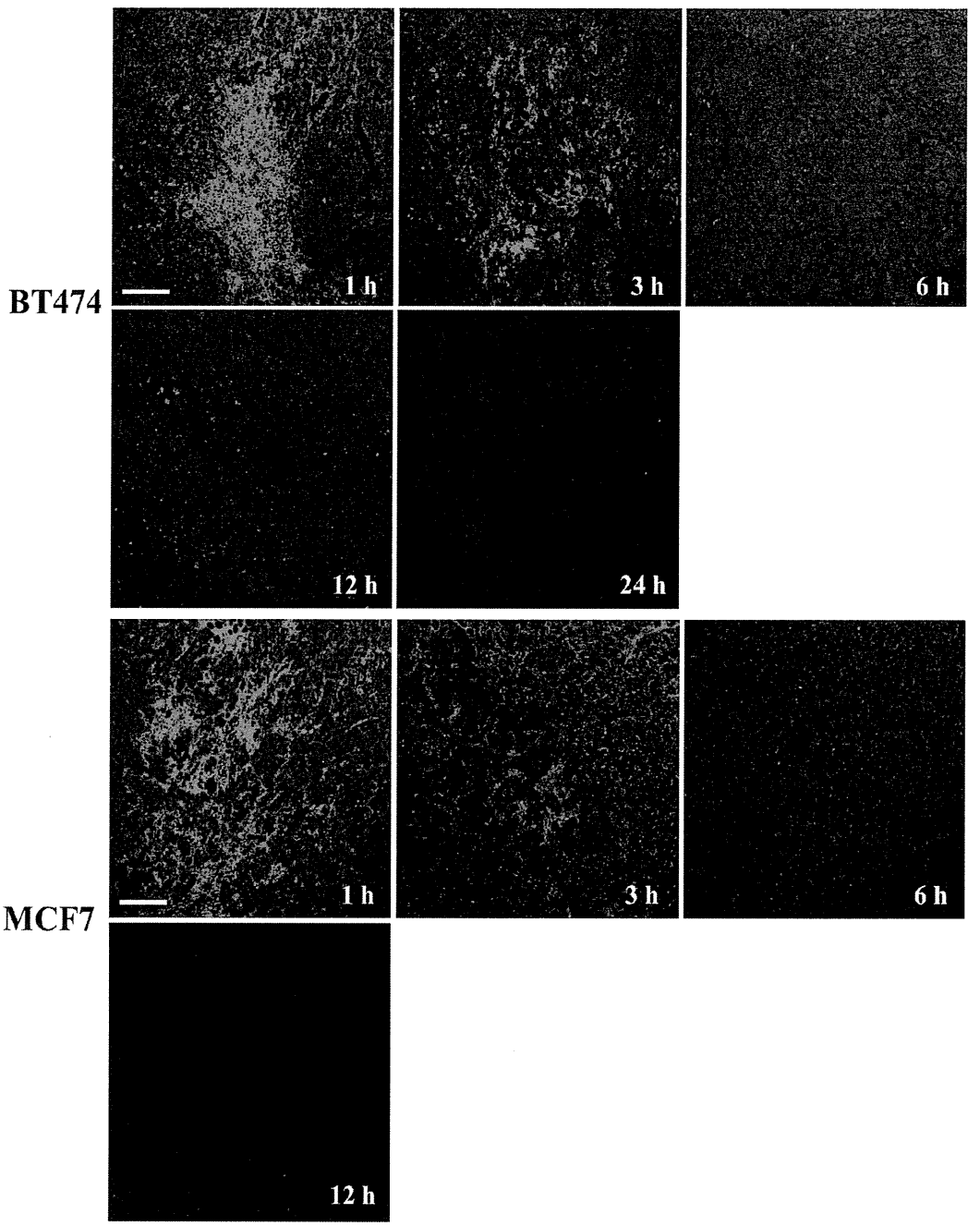

Fig.5. Han et al

Figure 5. Tumor site retention of EC1-GLuc-p53C after injection. At indicated time points after intratumoral injection of EC1-GLuc-p53C, mice were killed and tumors were excised. Tumors were then immediately fixed with 4% PFA. Paraffin-embedded slices of tumors were prepared at a thickness of 10 μm. Immunofluorescence staining with rabbit anti-*Gaussia* Luciferase serum was used to detect the retention of EC1-GLuc-p53C in tumors. Scale bars = 100 μm. n = 3 in each group.

doi: 10.1371/journal.pone.0075288.g005

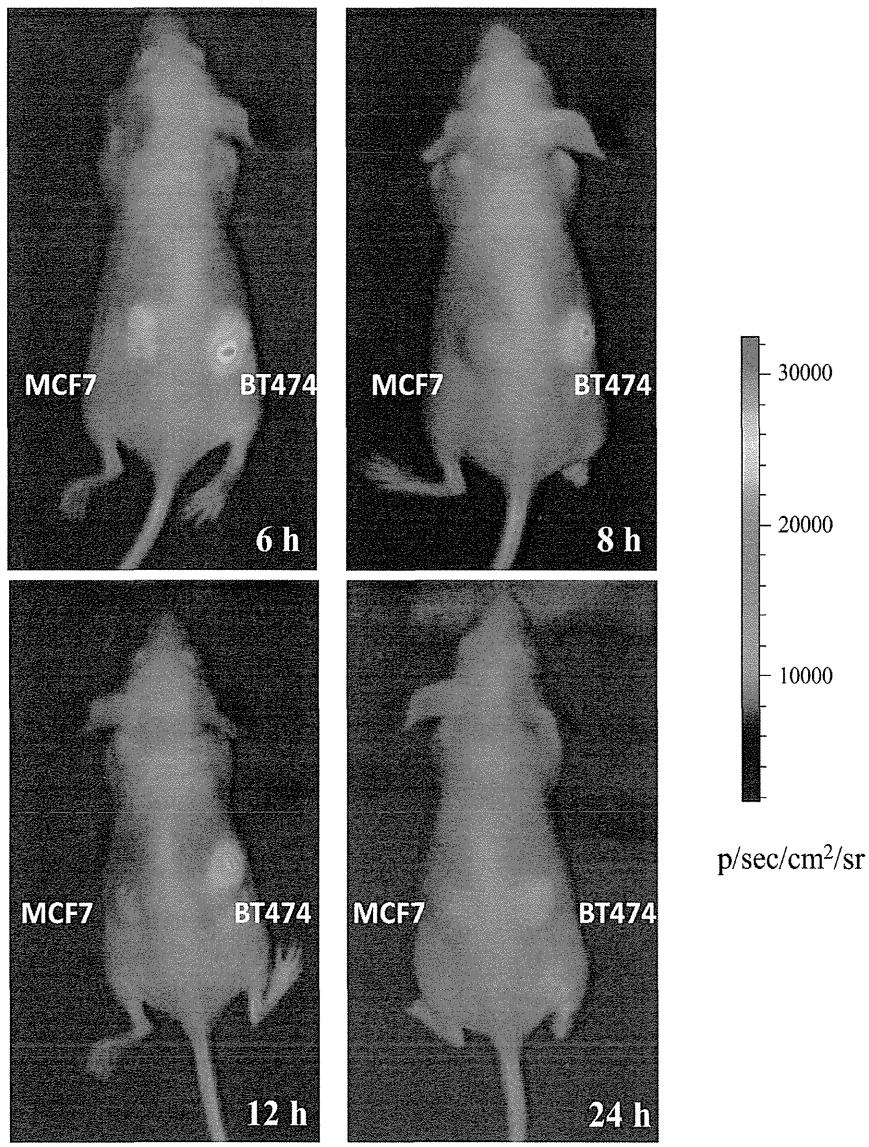

Fig.6. Han et al

Figure 6. Bioluminescence imaging in living nude mice bearing MCF7 and BT474 tumors. MCF7 and BT474 tumors were established on the left and right flank of nude mice, respectively. At 6, 8, 12 and 24 h after the application of EC1-GLuc-p53C, the mice were imaged immediately after the intravenous injection of CTZ solution (3mg/Kg). The color scale represents p/sec/cm²/ steradian. n = 3 in each group.

doi: 10.1371/journal.pone.0075288.g006

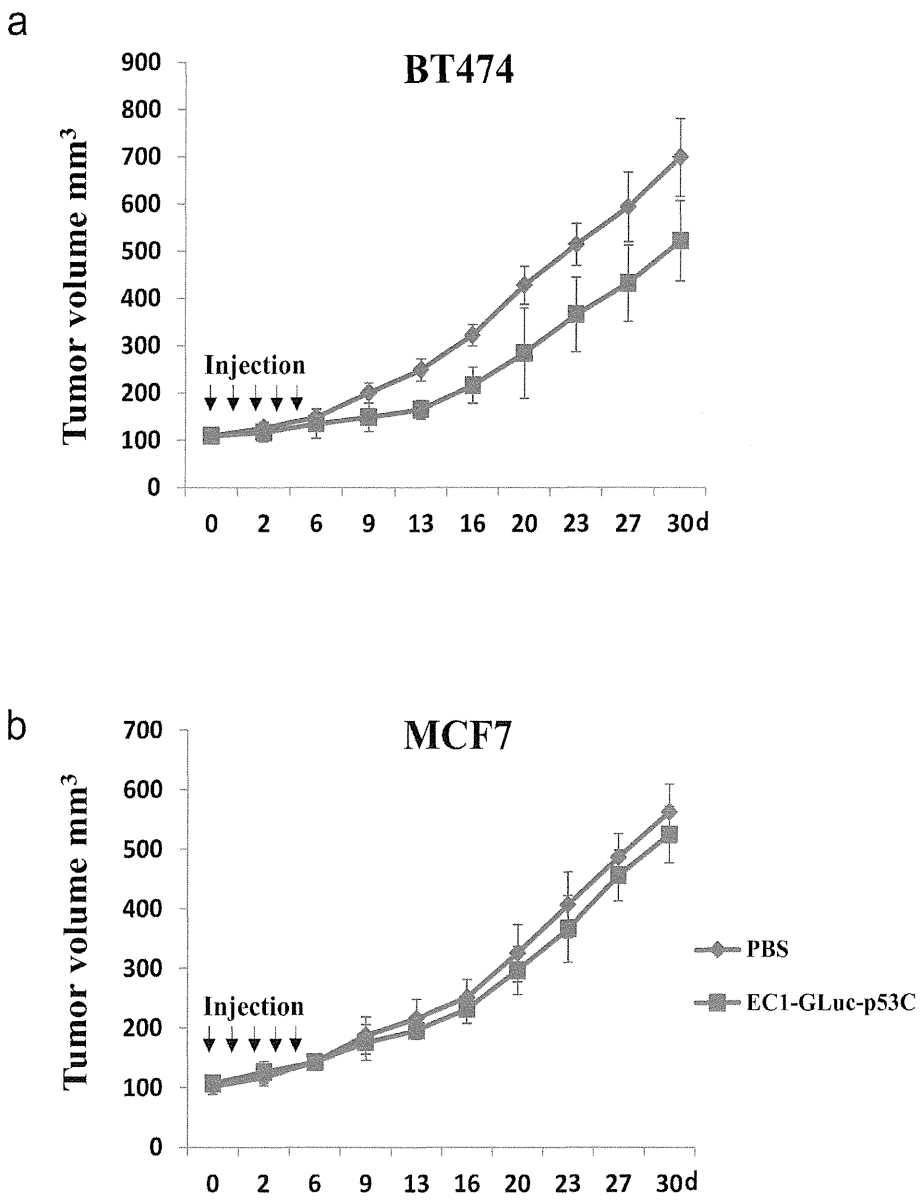

Fig.7. Han et al

Figure 7. Effect of EC1-GLuc-p53C on tumor growth. 30 μL of EC1-GLuc-p53C (0.5 μg/μL) or the same volume of PBS (control) were injected into MCF7 and BT474 tumors every day for 5 days. The mice were monitored daily and their tumor volume was measured twice a week to evaluate the effect of EC1-GLuc-p53C on tumor growth. n = 9 in each group.

doi: 10.1371/journal.pone.0075288.g007

[39,43]. In the present study, we designed a novel fusion protein for ErbB2-targeted imaging and cancer therapy. In the fusion protein, EC1 peptide, an artificial ErbB2 ligand, and a p53 reactivating peptide, p53C, were fused to *Gaussia* luciferase. We hypothesized that EC1-GLuc-p53C protein would exhibit the functions of all three components: targeting ErbB2, bioluminescence imaging and anticancer activity. *In vitro* assays showed that the bioluminescent activity of EC1-GLuc-p53C was reduced to approximately 50% of that of GLuc by the N- and C-terminal fusion of the two peptides. However, the bioluminescence of EC1-GLuc-p53C in serum was much more stable than that of GLuc (Figure 2a). At 3 h after incubation in serum, EC1-GLuc-p53C was nearly similar to GLuc in bioluminescence activity (Figure 2b). With the high quantum yield of GLuc [37] and improved stability by peptide fusion, EC1-GLuc-p53C is expected to be suitable for applications *in vivo*.

Unlike other members of the ErbB family, ErbB2 is an orphan receptor without an endogenous ligand. In a phage display study, an artificial peptide EC1 was found to bind to the extracellular domain of ErbB2 [14]. Importantly, the affinity for ErbB2 is retained in biotin-conjugated EC1, EC1-eGFP and EC1-Fc-liposome. In addition, EC1-fused molecules are selectively internalized into ErbB2-overexpressing cancer cells [14-16]. Consistent with previous studies, EC1-GLuc and EC1-GLuc-p53C also selectively targeted ErbB2-overexpressing BT474 cells (Figure 3b and Figure S1). These results suggest the ErbB2-targeting property of EC1 to be retained in our fusion proteins. On the other hand, it was reported that EC1 peptide at 25 and 50 μM inhibited the phosphorylation of ErbB2, and inhibited the growth of ErbB2-overexpressing MCF-7 cells at 1.0 μM [14]. However, we did not observe any significant effect of EC1-GLuc on the proliferation of BT474 cells at 1.0 μM. It is possible that EC1 suffers a loss in bioactivity when fused with GLuc. In contrast, EC1-GLuc-p53C significantly inhibited the proliferation of BT474, and its effect was dose-dependent (Figure 4a, b). Moreover, the p53C peptide in fusion protein was active and reactivated endogenous p53 when internalized in BT474 cells (Figure 4c). It indicates that the inhibitory effect of EC1-GLuc-p53C on cellular proliferation is due to the p53C peptide. Taken together, the *in vitro* results of the present study demonstrated that the three components in the newly designed fusion protein exerted their functions well.

For experiments *in vivo*, 50~75 μg of EC1-GLuc-p53C was injected into tumor-bearing mice via a tail vein, but no significant bioluminescence was detected in tumors at 0.5~12 h after the injection (data not shown). A previous study showed that an N-terminal truncated GLuc, GLΔ15 (20 kDa), was rapidly cleared through the kidneys over 20 min after its injection into mice, while the clearance of a diabody-fused GLΔ15 (90 kDa) was much slower [38]. We supposed that the small size of EC1-GLuc-p53C (25 kDa) might facilitate rapid clearance through the kidneys, and lead to very little accumulation of the fusion protein in tumors for bioluminescence imaging. Therefore, the intravenous injection was replaced with an intratumoral injection for experiments *in vivo*. The tumor site retention of EC1-GLuc-p53C showed that the fusion protein resided in BT474 tumors for up to 24 h after the intratumoral injection, whereas it was only weakly detected in MCF7 tumors up to 6 h (Figure 5), suggesting the longer retention time of EC1-GLuc-p53C in BT474 tumors to be due to its affinity for the ErbB2 receptor. Consistent with the retention of EC1-GLuc-p53C, bioluminescence was specifically detected in BT474 tumors from 8 h after protein injection (Figure 6). In addition, the repeated injection of EC1-GLuc-p53C selectively inhibited the growth of BT474 tumors (Figure 7), while no significant therapeutic effect was observed in BT474 tumors treated with PBS, GLuc or EC1-GLuc (Figure S3). The results suggest that EC1-GLuc-p53C is effective for the bioluminescence imaging and treatment of ErbB2-overexpressing tumors *in vivo*, although further optimization is needed for intravenous administration.

The combination of a diagnostic test and a therapeutic entity is termed theranostics [44,45]. In recent years, theranostics has developed very quickly along with selective targeting strategies. The targeting moieties include proteins (mainly antibodies and their fragments), peptides and some small molecules (folate and flavin mononucleotide) [45]. Peptides are attractive targeting molecules due to their small size, low immunogenicity and ease of manufacture at low costs. In the present research, we used EC1 peptide as a targeting moiety. The fusion protein EC1-GLuc-p53C efficiently targeted ErbB2-overexpressing cancer cells for bioluminescence imaging and therapy *in vitro* and *in vivo*. Thus, our multifunctional EC1 fusion protein should be a promising theranostic reagent for ErbB2-overexpressing tumors, although the development of this technology is still at the early stage. In addition, this system may also provide new theranostic reagents for other cancers with selective targeting moieties.

Conclusions

The present study showed the utility of a newly constructed protein, EC1-GLuc-p53C, for ErbB2-targeted bioluminescence imaging and cancer therapy *in vitro* and *in vivo*. EC1-GLuc-p53C retained the ErbB2-targeting property, and the enzymatic activity of GLuc in the fusion protein was successfully applied to the bioluminescence imaging of ErbB2-overexpressing BT474 cells *in vitro* and xenografted BT474 tumors *in vivo*; moreover, when internalized into cells, the p53C peptide in the fusion protein was active and exerted anticancer activity to inhibit tumor growth. In conclusion, EC1-GLuc-p53C may be a promising theranostic reagent for ErbB2-overexpressing cancer *in vitro* and *in vivo*.

Supporting Information

Figure S1. Bioluminescence imaging of cells treated with EC1-GLuc and GLuc *in vitro*. After incubation with 1 μM of EC-GLuc (c-d and g-h) or GLuc (a-b and e-f), MCF7 (a-d) and BT474 (e-h) cells were washed with culture medium without serum. Images were acquired with a bioluminescence microscope immediately after the addition of 1 μg/mL CTZ. Bars = 100 μm.
(TIF)

Figure S2. Confirmation of the established MCF7 and BT474 xenografted tumors. a) Histological observations of xenografted tumors were made using H&E staining. Bar = 1.0 mm. b) Expression of ErbB2 in MCF7 and BT474 tumors. Paraffin-embedded slices of tumors were subjected to IF staining with rabbit anti-ErbB2 antibody and Hoechst 33248 for nuclear staining. Bars = 100 μm. n = 3 in each group.
(TIF)

Figure S3. Therapeutic Effect of EC1-GLuc-p53C on tumor growth is derived from the efficacy of p53C. 30 μL of GLuc, EC1-GLuc, EC1-GLuc-p53C (0.5 μg/μL) or the same volume of PBS were injected into BT474 tumors every day for 5 days. Tumor volume was measured twice a week to monitor tumor growth. n = 7 in each group.
(TIF)

Author Contributions

Conceived and designed the experiments: XH KT. Performed the experiments: XH LS YN. Analyzed the data: XH BF. Contributed reagents/materials/analysis tools: H. Michiue MS H. Matsui. Wrote the manuscript: XH KT.

References

1. Tzahar E, Waterman H, Chen X, Levkowitz G, Karunagaran D et al. (1996) A hierarchical network of interreceptor interactions determines signal transduction by Neu differentiation factor/neuregulin and epidermal growth factor. Mol Cell Biol 16: 5276-5287. PubMed: 8816440.
2. Graus-Porta D, Beerli RR, Daly JM, Hynes NE (1997) ErbB-2, the preferred heterodimerization partner of all ErbB receptors, is a mediator of lateral signaling. EMBO J 16: 1647-1655. PubMed: 9130710.
3. Yarden Y, Sliwkowski MX (2001) Untangling the ErbB signalling network. Nat Rev Mol Cell Biol 2: 127-137. PubMed: 11252954.
4. Yu D, Hung MC (2000) Overexpression of ErbB2 in cancer and ErbB2-targeting strategies. Oncogene 19: 6115-6121. PubMed: 11156524.
5. Salomon DS, Brandt R, Ciardiello F, Normanno N (1995) Epidermal growth factor-related peptides and their receptors in human malignancies. Crit Rev Oncol/Hematol 19: 183-232. PubMed: 7612182.
6. Olayioye MA, Neve RM, Lane HA, Hynes NE (2000) The ErbB signaling network: receptor heterodimerization in development and cancer. EMBO J 19: 3159-3167. PubMed: 10880430.
7. Slamon DJ, Godolphin W, Jones LA, Holt JA, Wong SG et al. (1989) Studies of the HER-2/neu proto-oncogene in human breast and ovarian cancer. Science 244: 707-712. PubMed: 2470152.
8. Wang SC, Hung MC (2001) HER2 overexpression and cancer targeting. Semin Oncol 28: 115-124. PubMed: 11706403.
9. Berchuck A, Kamel A, Whitaker R, Kerns B, Olt G et al. (1990) Overexpression of HER-2/neu is associated with poor survival in advanced epithelial ovarian cancer. Cancer Res 50: 4087-4091. PubMed: 1972347.
10. Slamon DJ, Clark GM, Wong SG, Levin WJ, Ullrich A et al. (1987) Human breast cancer: correlation of relapse and survival with amplification of the HER-2/neu oncogene. Science 235: 177-182. PubMed: 3798106.
11. Kim R, Tanabe K, Uchida Y, Osaki A, Toge T (2002) The role of HER-2 oncoprotein in drug-sensitivity in breast cancer. Oncol Rep 9: 3-9. PubMed: 11748447.
12. Mitsunaga M, Ogawa M, Kosaka N, Rosenblum LT, Choyke PL et al. (2011) Cancer cell-selective *in vivo* near infrared photoimmunotherapy targeting specific membrane molecules. Nat Med 17: 1685-1691. PubMed: 22057348.
13. Govindarajan S, Sivakumar J, Garimidi P, Rangaraj N, Kumar JM et al. (2012) Targeting human epidermal growth factor receptor 2 by a cell-penetrating peptide-affibody bioconjugate. Biomaterials 33: 2570-2582. PubMed: 22192536.
14. Pero SC, Shukla GS, Armstrong AL, Peterson D, Fuller SP et al. (2004) Identification of a small peptide that inhibits the phosphorylation of ErbB2 and proliferation of ErbB2 overexpressing breast cancer cells. Int J Cancer 111: 951-960. PubMed: 15300809.
15. Hashizume T, Fukuda T, Nagaoka T, Tada H, Yamada H et al. (2008) Cell type dependent endocytic internalization of ErbB2 with an artificial peptide ligand that binds to ErbB2. Cell Biol Int 32: 814-826. PubMed: 18442934.
16. Vaidyanath A, Hashizume T, Nagaoka T, Takeyasu N, Satoh H et al. (2011) Enhanced internalization of ErbB2 in SK-BR-3 cells with multivalent forms of an artificial ligand. J Cell Mol Med 15: 2525-2538. PubMed: 21323863.
17. Haberkorn U, Markert A, Eisenhut M, Mier W, Altmann A (2011) Development of molecular techniques for imaging and treatment of tumors. Q J Nucl Med Mol Imaging 55: 655-670. PubMed: 22231585.
18. Vousden KH, Lu X (2002) Live or let die: the cell's response to p53. Nat Rev Cancer 2: 594-604. PubMed: 12154352.
19. Foster BA, Coffey HA, Morin MJ, Rastinejad F (1999) Pharmacological rescue of mutant p53 conformation and function. Science 286: 2507-2510. PubMed: 10617466.
20. Bykov VJ, Issaeva N, Shilov A, Hultcrantz M, Pugacheva E et al. (2002) Restoration of the tumor suppressor function to mutant p53 by a low-molecular-weight compound. Nat Med 8: 282-288. PubMed: 11875500.
21. Michiue H, Tomizawa K, Wei FY, Matsushita M, Lu YF et al. (2005) The NH2 terminus of influenza virus hemagglutinin-2 subunit peptides enhances the antitumor potency of polyarginine-mediated p53 protein transduction. J Biol Chem 280: 8285-8289. PubMed: 15611109.
22. Takenobu T, Tomizawa K, Matsushita M, Li ST, Moriwaki A et al. (2002) Development of p53 protein transduction therapy using membrane-permeable peptides and the application to oral cancer cells. Mol Cancer Ther 1: 1043-1049. PubMed: 12481427.
23. Inoue M, Tomizawa K, Matsushita M, Lu YF et al. (2006) p53 protein transduction therapy: successful targeting and inhibition of the growth of the bladder cancer cells. Eur Urol 49: 161-168. PubMed: 16310931.
24. Michael D, Oren M (2003) The p53-Mdm2 module and the ubiquitin system. Semin Cancer Biol 13: 49-58. PubMed: 12507556.
25. Bode AM, Dong Z (2004) Post-translational modification of p53 in tumorigenesis. Nat Rev Cancer 4: 793-795. PubMed: 15510160.
26. Olsson A, Manzl C, Strasser A, Villunger A (2007) How important are posttranslational modifications in p53 for selectivity in target-gene transcription and tumour suppression? Cell Death Differ 14: 1561-1565. PubMed: 17627286.
27. Hupp TR, Sparks A, Lane DP (1995) Small peptides activate the latent sequence-specific DNA binding function of p53. Cell 83: 237-245. PubMed: 7585941.
28. Kim AL, Raffo AJ, Brandt-Rauf PW, Pincus MR, Monaco R et al. (1999) Conformational and molecular basis for induction of apoptosis by a p53 C-terminal peptide in human cancer cells. J Biol Chem 274: 34924-34931. PubMed: 10574967.
29. Snyder EL, Meade BR, Saenz CC, Dowdy SF (2004) Treatment of terminal peritoneal carcinomatosis by a transducible p53-activating peptide. PLOS Biol 2: 0186-0193. PubMed: 14966535.
30. Araki D, Takayama K, Inoue M, Watanabe T, Kumon H et al. (2010) Cell-penetrating D-isomer peptides of p53 C-terminus: long-term inhibitory effect on the growth of bladder cancer. Urology 75: 813-819. PubMed: 19963248.
31. Takayama K, Nakase I, Michiue H, Takeuchi T, Tomizawa K et al. (2009) Enhanced intracellular delivery using arginine-rich peptides by the addition of penetration accelerating sequences (Pas). J Control Release 138: 128-133. PubMed: 19465072.
32. Tannous BA (2009) Gaussia luciferase reporter assay for monitoring biological processes in culture and *in vivo*. Nat Protoc 4: 582-591. PubMed: 19373229.
33. Dothager RS, Flentie K, Moss B, Pan MH, Kesarwala A et al. (2009) Advances in bioluminescence imaging of live animal models. Curr Opin Biotechnol 20: 45-53. PubMed: 19233638.
34. Lembert N, Idahl LA (1995) Regulatory effects of ATP and luciferin on firefly luciferase activity. Biochem J 305: 929-933. PubMed: 7848294.
35. Matthews JC, Hori K, Cormier MJ (1977) Substrate and substrate analogue binding properties of Renilla luciferase. Biochemistry 16: 5217-5220. PubMed: 21679.

36. Lorenz WW, McCann RO, Longiaru M, Cormier MJ (1991) Isolation and expression of a cDNA encoding Renilla reniformis luciferase. Proc Natl Acad Sci U S A 88: 4438-4442. PubMed: 1674607.
37. Tannous BA, Kim DE, Fernandez JL, Weissleder R, Breakefield XO (2005) Codon-optimized Gaussia luciferase cDNA for mammalian gene expression in culture and *in vivo*. Mol Ther 11: 435-443. PubMed: 15727940.
38. Venisnik KM, Olafsen T, Gambhir SS, Wu AM (2007) Fusion of *Gaussia* luciferase to an engineered anti-carcinoembryonic antigen (CEA) antibody for *in vivo* optical imaging. Mol Imaging Biol 9: 267-277. PubMed: 17577599.
39. Feng B, Tomizawa K, Michiue H, Han XJ, Miyatake S et al. (2010) Development of a bifunctional immunoliposome system for combined drug delivery and imaging *in vivo*. Biomaterials 31: 4139-4145. PubMed: 20149431.
40. Funkhouser J (2002) Reinventing pharma: The theranostic revolution. Current Drugs Discov 2: 17-19.
41. Ding H, Wu F (2012) Image Guided Biodistribution and Pharmacokinetic Studies of Theranostics. Theranostics 2: 1040-1053. doi:10.7150/thno.4652. PubMed: 23227121.
42. Jia LQ, Osada M, Ishioka C, Gamo M, Ikawa S et al. (1997) Screening the p53 status of human cell lines using a yeast functional assay. Mol Carcinog 19: 243-253. PubMed: 9290701.
43. Feng B, Tomizawa K, Michiue H, Miyatake S, Han XJ et al. (2009) Delivery of sodium borocaptate to glioma cells using immunoliposome conjugated with anti-EGFR antibodies by ZZ-His. Biomaterials 30: 1746-1755. PubMed: 19121537.
44. Del Vecchio S, Zannetti A, Fonti R, Pace L, Salvatore M (2007) Nuclear imaging in cancer theranostics. Q J Nucl Med Mol Imaging 51: 152-163. PubMed: 17420716.
45. Yu MK, Park J, Jon S (2012) Targeting strategies for multifunctional nanoparticles in cancer imaging and therapy. Theranostics 2: 3-44. PubMed: 22272217.

NEOPLASIA
www.neoplasia.com

Volume 15 Number 11 November 2013 pp. 1272–1281 1272

Cyclin G2 Promotes Hypoxia-Driven Local Invasion of Glioblastoma by Orchestrating Cytoskeletal Dynamics[1,2]

Atsushi Fujimura*,†, Hiroyuki Michiue*, Yan Cheng*, Atsuhito Uneda*, Yasunari Tani*, Tei-ichi Nishiki*, Tomotsugu Ichikawa‡, Fan-Yan Wei§, Kazuhito Tomizawa§ and Hideki Matsui*

*Department of Physiology, Okayama University Graduate School of Medicine, Dentistry and Pharmaceutical Sciences, Okayama, Japan; †Advanced Research Training Program, Okayama University Graduate School of Medicine, Dentistry and Pharmaceutical Sciences, Okayama, Japan; ‡Department of Neurosurgery, Okayama University Hospital, Okayama, Japan; §Department of Molecular Physiology, Faculty of Life Sciences, Kumamoto University, Kumamoto, Japan

Abstract

Microenvironmental conditions such as hypoxia potentiate the local invasion of malignant tumors including glioblastomas by modulating signal transduction and protein modification, yet the mechanism by which hypoxia controls cytoskeletal dynamics to promote the local invasion is not well defined. Here, we show that cyclin G2 plays pivotal roles in the cytoskeletal dynamics in hypoxia-driven invasion by glioblastoma cells. Cyclin G2 is a hypoxia-induced and cytoskeleton-associated protein and is required for glioblastoma expansion. Mechanistically, cyclin G2 recruits cortactin to the juxtamembrane through its SH3 domain–binding motif and consequently promotes the restricted tyrosine phosphorylation of cortactin in concert with src. Moreover, cyclin G2 interacts with filamentous actin to facilitate the formation of membrane ruffles. In primary glioblastoma, cyclin G2 is abundantly expressed in severely hypoxic regions such as pseudopalisades, which consist of actively migrating glioma cells. Furthermore, we show the effectiveness of dasatinib against hypoxia-driven, cyclin G2–involved invasion *in vitro* and *in vivo*. Our findings elucidate the mechanism of cytoskeletal regulation by which severe hypoxia promotes the local invasion and may provide a therapeutic target in glioblastoma.

Neoplasia (2013) 15, 1272–1281

Introduction

Glioblastoma multiforme (GBM), the most common and malignant primary tumor arising in the central nervous system, is characterized by a variety of pathologic findings including vascular proliferation, aggressive invasion, and pseudopalisades [1], which are promoted by hypoxic conditions [2,3]. Pseudopalisades consist of necrotic foci and surrounding glioma cells and are a specific finding that distinguishes GBM from lower grade astrocytomas [4]. They were also shown to consist of hypoxic and actively migrating glioma cells [5].

In the expansion of GBM, hypoxia contributes to the maintenance of glioma stem cells, angiogenesis, and cellular migration through the accumulation of hypoxia-inducible factor 1α (HIF-1α) and consequent activation of several genes [6–8]. Studies using microarray-based gene expression profiling in glioma or neuroblastoma cells have

Address all correspondence to: Dr Hiroyuki Michiue, MD, PhD, 2-5-1 Shikata-cho, Kita-ku, Okayama City, Okayama Prefecture, Japan. E-mail: hmichiue@md.okayama-u.ac.jp

[1]This work is supported by a Grant-in-aid for Scientific Research from the Ministry of Education, Science, Sports and Culture of Japan, by Okinaka Memorial Institute for Medical Research, and by a Grant-in-aid for Scientific Research from the Ministry of Health, Labor and Welfare of Japan. A.F. is supported by the Advanced Research Training Program (Okayama University Hospital) and Sekizenkai, a foundation of Okayama University Hospital. The authors declare no competing financial interests.
[2]This article refers to supplementary materials, which are designated by Figures W1 to W8 and are available online at www.neoplasia.com.
Received 7 August 2013; Revised 21 October 2013; Accepted 21 October 2013

DOI 10.1593/neo.131440

indicated the knockdown of HIF-1α to result in reduced expression of *ccng2* mRNA (which encodes cyclin G2), suggesting that cyclin G2 expression is hypoxia-responsive [9–11]. Cyclin G2 was first identified as a negative regulator of cell cycle progression [12] and shown to bind to an active complex of protein phosphatase 2A (PP2A) and induce a p53-dependent cell cycle arrest [13]. Moreover, cyclin G2 interacts with and stabilizes microtubules, suggesting that cyclin G2 contributes to the regulation of cytoskeletal dynamics [13]. Despite evidence that the expression and subcellular distribution of cyclin G2 were related to epithelial cancer progression and metastasis [14–16], the precise mechanism by which cyclin G2 controls tumor expansion is unclear, especially in GBM.

Although several studies have shown that hypoxia induced by tumor enlargement or antiangiogenic therapy stimulated the local invasion of glioblastoma cells by modulating signal transduction [8], we do not have sufficient evidence that hypoxia regulates cytoskeletal dynamics, which is required for cellular motility, to promote the local invasion of glioblastoma. Accordingly, the aim of this study is to elucidate the precise mechanism of cytoskeletal regulation in the hypoxia-driven invasion and thereby provide evidence of a therapeutic strategy in glioblastoma. Especially, we here focus on the roles of cyclin G2 in cellular migration in response to hypoxia from the viewpoint of cytoskeletal regulation.

Materials and Methods

Cell Culture and Reagents

Human glioma cell lines U87MG, U251MG, and LNZ308 and human embryonic kidney (HEK) 293 cells were cultured in Dulbecco's modified Eagle's medium (DMEM) with 10% FBS and penicillin/streptomycin (Life Technologies, Carlsbad, CA). Murine glioma-initiating 005 cells were cultured as previously reported [17]. For hypoxic stimulation, cells were cultured in medium containing 100 μM deferoxamine mesylate (Sigma-Aldrich, St Louis, MO) or hypoxic chamber maintained at 5% or 1% O_2. For the analysis of tyrosine phosphorylation, 10 μM erlotinib (LKT Laboratories, Inc, St Paul, MN) or 1 μM dasatinib (Selleck Chemicals, Houston, TX) was added before the hypoxic stimulation (Figure W7).

For the immunoblot analysis, the following antibodies were used as the primary antibody: anti–cyclin G2, anti-Src, anti-p21, anti-p53, anti-green fluorescent protein (GFP; Santa Cruz Biotechnology, Inc, Dallas, TX), anti–HIF-1α (Novus Biologicals, LLC, Littleton, CO), anti–α-tubulin, anti–β-actin (Sigma-Aldrich), anti-cortactin, anti-phosphotyrosine (Millipore, Billerica, MA), and anti-Src (Cell Signaling Technology, Inc, Danvers, MA). For the immunohistochemistry and immunofluorescence, the following antibodies were used: anti–cyclin G2, anti-Src, anti-CD68 (Santa Cruz Biotechnology, Inc), anti–HIF-1α (Novus Biologicals, LLC), anti-human glial fibrillary acidic protein (GFAP), anti-cortactin (Abcam, Cambridge, United Kingdom), anti–α-tubulin (Sigma-Aldrich), anti-cortactin, anti-phosphotyrosine (Millipore), and anti–phospho-Src (Y417) (Life Technologies). Alexa Fluor 555–conjugated phalloidin and Hoechst (Life Technologies) were used for the detection of F-actin and nuclei, respectively. Validation of the use of the cyclin G2 antibody in immunoblot, immunofluorescent, and immunostaining analyses was reported in the past studies [14,18,19] and was further confirmed as shown in Figure W7.

For the analysis of cell proliferation and viability, the water soluble tetrazolium-1 (WST-1) assay was performed according to the manufacturer's protocol (Roche, Tokyo, Japan).

Luciferase Reporter Assay

The human cyclin G2 promoter region (−1600~0) was amplified from genomic DNA of U87MG cells and cloned into a pGL4.14 luciferase reporter vector (Promega, Madison, WI). The vectors were transfected into U87MG cells before hypoxic stimulation and cultured in a hypoxic chamber for 24 hours. The cells were lysed and incubated with the Luciferase Assay System (Promega) before measurements were made. Oligonucleotides for amplification of human cyclin G2 promoter region were given as follows: forward, 5′-CAAAACCCTCACCAAGCTCACACCTCTCTG-3′; reverse, 5′-CCCCTTGTTTTTGTTAAGAGTTTCGACGCC-3′.

Wound-Healing Assay

Cells were plated on Matrigel-coated glass slips at 90% confluence and cultured for 24 hours in DMEM with 10% FBS. The next day, the slips were scratched with white tips (200 μl), and the medium was switched to DMEM with 0.1% FBS. Then, the cells were incubated in normoxic or hypoxic conditions for 24 hours and observed. To examine the effects of ectopic expression of cyclin G2 on cellular motility, plasmids encoding cyclin G2–enhanced green fluorescent protein (EGFP), EGFP, $G2^{K219Q}$-EGFP, or $G2^{P291A}$-EGFP were transfected before the scratching.

Plasmids, Small Interfering RNA, and Retroviruses

The human cyclin G2 cDNA was purchased from OriGene (Rockville, MD; Cat. No. SC117452), and the open reading frame was cloned into a pEGFP-N3 (Clontech, Mountain View, CA) or a pcDNA3.1/V5-His TOPO vector (Life Technologies). The K219Q and P291A mutants were generated using the site-directed mutagenesis kit (Stratagene, La Jolla, CA). Small interfering RNA (siRNA) and scrambled RNA were obtained from Thermo Fisher Scientific Inc (Waltham, MA; Dharmacon, ON-TARGET*plus* siRNA Reagents). The retrovirus encoding scrambled shRNA or shRNA against human *ccng2* was prepared using the HuSH-29 plasmids (OriGene) and PT67 cells (Clontech) according to the manufacturer's recommendation.

RNA Purification, cDNA Synthesis, and Real-Time Reverse Transcription–Polymerase Chain Reaction

For reverse transcription–polymerase chain reaction (PCR) analysis, total RNA was isolated from GBM and cancer cells using an RNeasy kit (Qiagen, Santa Clarita, CA) and subjected to on-column digestion of genomic DNA with RNase-free DNase (TaKaRa, Otsu, Japan). With 1 μg of purified total RNA, cDNA was synthesized using a Maxima cDNA synthesis kit (Thermo Fisher Scientific Inc) Quantitative analyses of *CCNG2*, *FYN*, *CSK*, *SRC*, *LYN*, and *LCK* mRNA were performed with RT^2 SYBR Green master mixes (Qiagen) and the ABI PRISM 7000 Sequence Detection System (Life Technologies). As an internal control, the copy number of *ACTB* (β-actin) mRNA was determined. We obtained predesigned and certified primers from TaKaRa. All data were analyzed using software (7000v1.1; Life Technologies).

Western Blot Analysis and Preparation of Cytoskeletal Pellets

Immunoblot analysis was performed as described previously [20]. Cells were lysed in cell lysis buffer [20 mM Tris-HCl (pH 7.5), 150 mM NaCl, 1 mM EDTA, 1 mM EGTA, and 0.5% Triton X-100) containing Complete Proteinase Inhibitor Cocktail (Roche). For the detection of phosphoprotein, PhosSTOP Phosphatase Inhibitor Cocktail (Roche)

was added. Samples were subjected to sodium dodecyl sulfate (SDS)–polyacrylamide gel electrophoresis, blotted on a nitrocellulose membrane, and subjected to immunodetection. HRP signals were visualized using Chemiluminescent Peroxidase Substrates (Sigma-Aldrich) and detected by VersaDoc (Bio-Rad, Hercules, CA). Signal density was analyzed using the VersaDoc software. All raw data are shown in Figure W8.

For preparing a cytoskeletal fraction mainly containing filamentous actin, we used a G-actin/F-actin *In Vivo* Assay Biochem Kit (Cytoskeleton, Inc) with minor modifications. Briefly, EGFP-, cyclin G2–EGFP–, or $G2^{K219Q}$-EGFP–transfected U87MG cells were incubated with phalloidin (1 μg/ml) and nocodazole (200 ng/ml) for 2 hours before the fractionation of filamentous actin with the kit. For the microtubule pellet, the cells were incubated with latrunculin B (250 ng/ml) and paclitaxel (500 ng/ml) for 2 hours and lysed with microtubule stabilization buffer [50 mM Pipes (pH 6.9), 5 mM $MgCl_2$, 2 mM EGTA, 0.1% Triton X-100, 0.1% NP-40, 100 μM GTP, 1 mM ATP, 250 ng/ml latrunculin B, 500 ng/ml paclitaxel] before fractionation by ultracentrifuge (100,000*g*).

Immunohistochemistry and Immunofluorescence

Paraffin-embedded human GBM specimens were prepared in the Okayama University Hospital's Department of Pathology. Sections were deparaffinized, epitope-retrieved with proteinase XXV (Thermo Scientific), and blocked with 5% donkey serum in phosphate-buffered saline (Abcam). Slides were incubated at 4°C for 16 hours with primary antibodies, visualized with the ImmPRESS polymerized enzyme staining kit (VECTOR Laboratories, Burlingame, CA), and counterstained with hematoxylin. For the immunofluorescent analysis of human GBM specimens, sections were prepared as described above except for the secondary antibodies (Life Technologies; Alexa Fluor 488– or Alexa Fluor 555–conjugated antibodies). For the immunofluorescent analyses of glioma cell lines, cells were fixed with 4% paraformaldehyde (PFA) for 15 minutes, permeated with 0.2% Triton X-100 for 10 minutes, and blocked with 5% goat (Abcam) or donkey serum. The samples were then incubated with primary antibodies and secondary antibodies. Immunofluorescent samples were observed with a confocal laser scanning microscope (FluoView 300; Olympus, Tokyo, Japan).

Immunoprecipitation and Chromatin Immunoprecipitation Assay

To investigate the interaction between cyclin G2, cortactin, and src family kinases (SFKs), plasmids encoding EGFP, EGFP-tagged cyclin G2, or the EGFP-tagged cyclin G2 mutant were transfected into U87MG cells using Lipofectamine 2000 according to the manufacturer's instructions (Life Technologies). After 20 hours, cells were lysed with immunoprecipitation (IP) buffer [20 mM Tris-HCl (pH 7.5), 150 mM NaCl, 1% Triton X-100, and proteinase inhibitor cocktail] and centrifuged. The supernatant was precleaned with protein G sepharose, incubated with anti-GFP antibody, and precipitated with protein G sepharose. Precipitated samples were boiled in 2× SDS buffer. For detection of phosphotyrosine, hypoxia-stimulated or cyclin G2–transfected U87MG cells were lysed in IP buffer containing PhosSTOP (Roche) and immunoprecipitated with anti-cortactin antibody.

For chromatin immunoprecipitation (ChIP) assay, 5×10^7 U87MG cells (cultured in normoxic or hypoxic conditions for 24 hours) were incubated with formaldehyde (final concentration of 0.75%) at room temperature for 15 minutes and lysed with lysis buffer [50 mM Hepes (pH 7.5), 140 mM NaCl, 1 mM EDTA, 1% Triton X-100, 0.1% sodium deoxycholate, 0.1% SDS, protease inhibitor]. After sonication, DNA concentrations of the samples were determined and the samples containing 25 μg of DNA were immunoprecipitated with anti–HIF1-α antibody or control mouse IgG, followed by PCR. Oligonucleotides for the ChIP assay were given as follows: HIF-1α—forward, 5′-CTCTTCCCAGGGACTATCTG-3′; reverse, 5′-GACTGAAGGAGGGGCTTTTC-3′.

Statistical Analysis

Data were analyzed either by Student's *t* test to identify significant differences between two groups or by Scheffe's posttest following a two-way analysis of variance to compare multiple groups. *P* values less than .05 were considered significant.

Results

Cyclin G2: A Marker of Pseudopalisades

To unveil the mechanism by which hypoxia regulates cytoskeletal dynamics, we first sought hypoxia-induced and cytoskeleton-associated proteins. According to past microarray studies in glioblastoma [9–11] and the ELM database analysis [21], we predicted cyclin G2 as a candidate (Figure W1, *A–D*). Cyclin G2 expression was commonly upregulated among three subsets of microarray data in hypoxia-treated glioblastoma or hypoxic region of GBM, and it was positively correlated with hypoxia signature (hypoxia-responsive genes, e.g., *ANGPTL4* and *HK2*) [22,23] also in the other array data set (Figure W1, *B* and *C*); the ELM program predicted that cyclin G2 had a putative SH2 domain–binding motif in the N terminus, an actin-interacting WH2 motif, and an SH3 domain–binding motif in the C terminus (Figure W1*D*). In fact, cyclin G2 expression was significantly increased in glioblastoma-derived cell lines in response to hypoxic stimulations (Figure 1, *A* and *B*). In the human *ccng2* (which encodes cyclin G2 protein) promoter region, we found some putative hypoxia-responsive elements (HREs; -CGTG-; Figure W2) [24]. Through luciferase reporter assays using the human *ccng2* promoter region and ChIP, we revealed that cyclin G2 expression was directly regulated by HIF-1α (Figure 1, *C* and *D*). Knockdown of HIF-1α by RNA interference caused a deficit of the hypoxia-induced cyclin G2 expression (Figure 1*E* and data not shown). Interestingly, p53, which affects the malignancy of glioblastoma, had no relationship to cyclin G2 expression (U87MG, $p53^{WT}$; U251MG, $p53^{Mut}$; LNZ308, $p53^{Null}$, respectively), and the forced expression of p53 had no effect on cyclin G2 expression (Figure W3*A*). In primary glioblastoma, we detected immunoreactive signals for cyclin G2 in the cytoplasm of glioma cells, not in inflammatory cells (CD68 positive), in hypoxic regions such as pseudopalisades, whereas no signal was observed in high cellularity/mitotic regions (Figures 1, *F–R*, and W4, *A–D*).

Cyclin G2 is an unconventional cyclin, which interacts with an active complex of PP2A and induces cell cycle arrest [12]. Recent studies indicated cyclin G2 to be involved in the progression of oral squamous cell carcinoma [14] and breast carcinoma [15,16]. In breast cancer, cyclin G2 was defined as a marker of suppression of invasion and metastasis under the control of TAp63, a well-known regulator of carcinoma expansion. However, the mechanism by which cyclin G2 determines cellular behavior is completely unclear. Importantly, cyclin G2 expression is enhanced by a variety of transcriptional molecules such as FoxO3a [25,26], Nodal-ALK4/7 [27], and HIF-1α (as shown in Figure 1), which are all known as key promoters of glioblastoma expansion. Combined with our findings

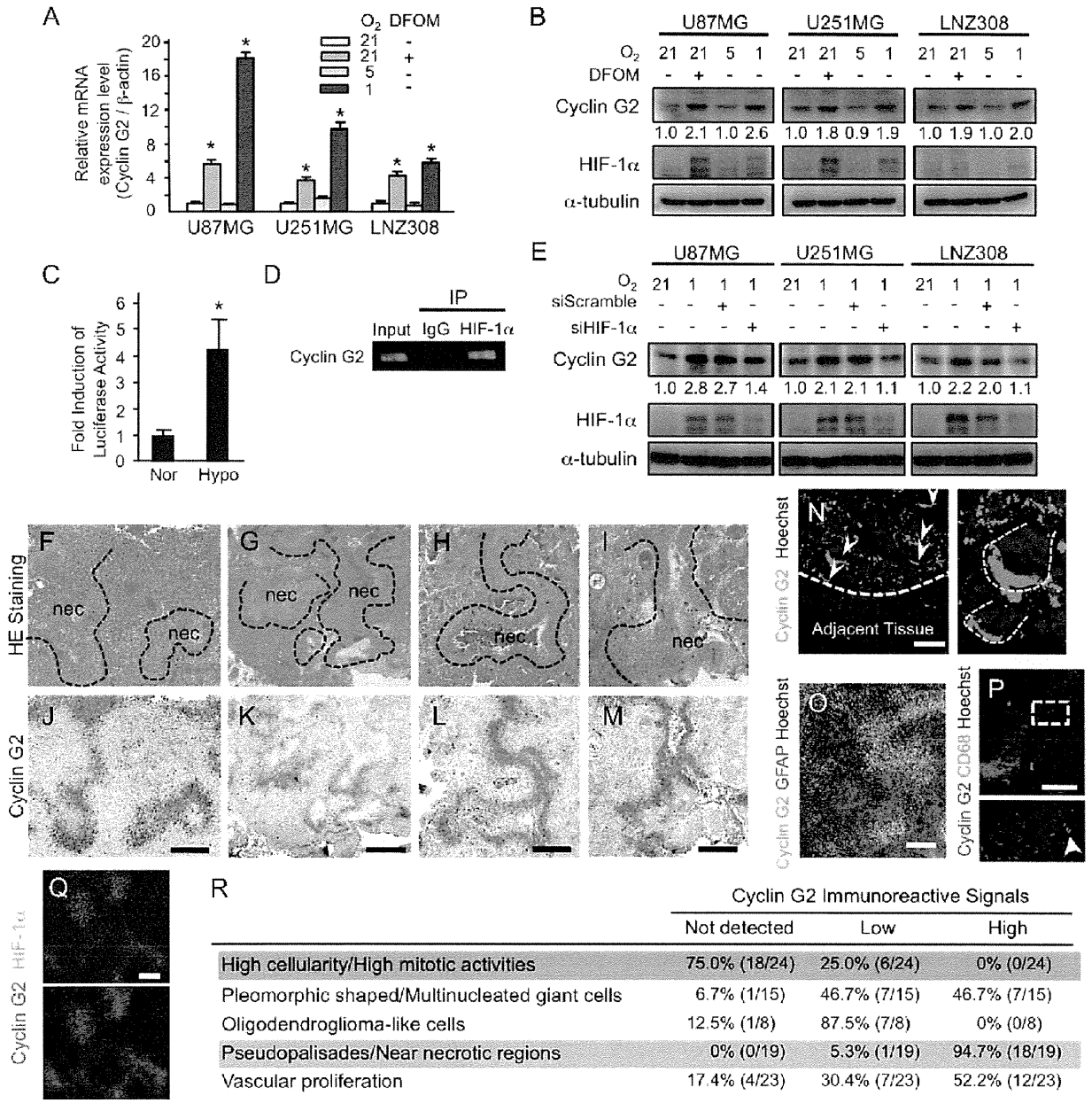

	Cyclin G2 Immunoreactive Signals		
	Not detected	Low	High
High cellularity/High mitotic activities	75.0% (18/24)	25.0% (6/24)	0% (0/24)
Pleomorphic shaped/Multinucleated giant cells	6.7% (1/15)	46.7% (7/15)	46.7% (7/15)
Oligodendroglioma-like cells	12.5% (1/8)	87.5% (7/8)	0% (0/8)
Pseudopalisades/Near necrotic regions	0% (0/19)	5.3% (1/19)	94.7% (18/19)
Vascular proliferation	17.4% (4/23)	30.4% (7/23)	52.2% (12/23)

Figure 1. Cyclin G2 is a hypoxia-induced protein and abundant in pseudopalisade-forming glioma cells. (A and B) Hypoxic conditions enhance *ccng2* mRNA transcription (A) and cyclin G2 protein expression (B). Cells were cultured in normoxic, deferoxamine mesylate (a reagent to mimic hypoxia)–added, or hypoxic conditions for 24 hours and subjected to reverse transcription–PCR or Western blot analysis. (C) Luciferase reporter assay with the human *ccng2* promoter/pGL4.14 vector. U87MG cells were transfected with the reporter vector and cultured in normoxic or hypoxic conditions for 24 hours. Bars represent the SD. (D) ChIP assay showing that cyclin G2 expression is directly regulated by HIF-1α. (E) Cyclin G2 expression is dependent on HIF-1α accumulation. Cells treated with siRNA against HIF-1α show lower expression of cyclin G2 than scrambled siRNA-treated cells under hypoxic conditions. (F–M) Human glioblastoma specimens stained with hematoxylin and eosin (H&E) and immunostained with anti–cyclin G2 antibody. Other images are shown in Figure W4. (N) Cyclin G2 accumulates at the leading edge of glioma cells migrating from the necrotic foci to adjacent tissue. (O and P) Cyclin G2 is abundant in pseudopalisade-forming glioma cells (O) but not in inflammatory cells (CD68 positive) (P). (Q and R) Cyclin G2 expression is abundant in hypoxic or near necrotic regions. Dotted lines indicate the borders of pseudopalisades (F–I). The scale bars represent 200 μm (J–M), 50 μm (N), 100 μm (O and P), respectively. Numbers in B and E represent the ratio of densitometry analysis.

that cyclin G2 is abundantly expressed in pseudopalisades, which consist of actively migrating glioma cells [4,5], we assumed that cyclin G2 had promotive effects on tumor expansion in glioblastoma, especially the hypoxia-driven local invasion, unlikely breast cancer.

Cyclin G2 Promotes GBM Migration

To test our hypothesis, we first investigated the role of cyclin G2 in the motility of glioblastoma cells. Wound-healing assays showed that hypoxia promoted the migration of glioblastoma cells (Figure 2*A*). As expected, the ectopically expressed cyclin G2 promoted migration of U87MG and U251MG cells even under normoxic conditions (Figure 2, *B–E*). To confirm this, we prepared cyclin G2–reduced U87MG and U251MG cells using a retroviral vector encoding shRNA against human *ccng2* (Figure 2*F*). The reduction in cyclin G2 caused excessive cell proliferation and p21 suppression, maybe because of the lack of cell cycle–inhibiting potential of cyclin G2 (Figure W3, *B* and *C*). Moreover, the shRNA-treated U87MG cells were flat and epithelia-like, unlike the spindle-shaped control cells (Figure 2*G*). Through wound-healing assays and single-cell tracing, we found that reduced expression of cyclin G2 caused the decrease in migration and cellular motility (Figure 2, *H–J*). In past studies, antiangiogenic treatment promoted the local invasion of glioblastoma cells by inducing hypoxic conditions [8]. According to our findings, cyclin G2 was involved in this. To verify this assumption, we intracranially implanted shRNA-treated U251MG cells into immunodeficient mice and treated them with CBO-P11, a vascular endothelial growth factor inhibitor. As previously reported [28], CBO-P11 reduced the cell density of the tumor core but promoted the local invasion of the cells treated with scrambled shRNA (Figure 2, *K–P*). In contrast, in cyclin G2–reduced U251MG cells, the local

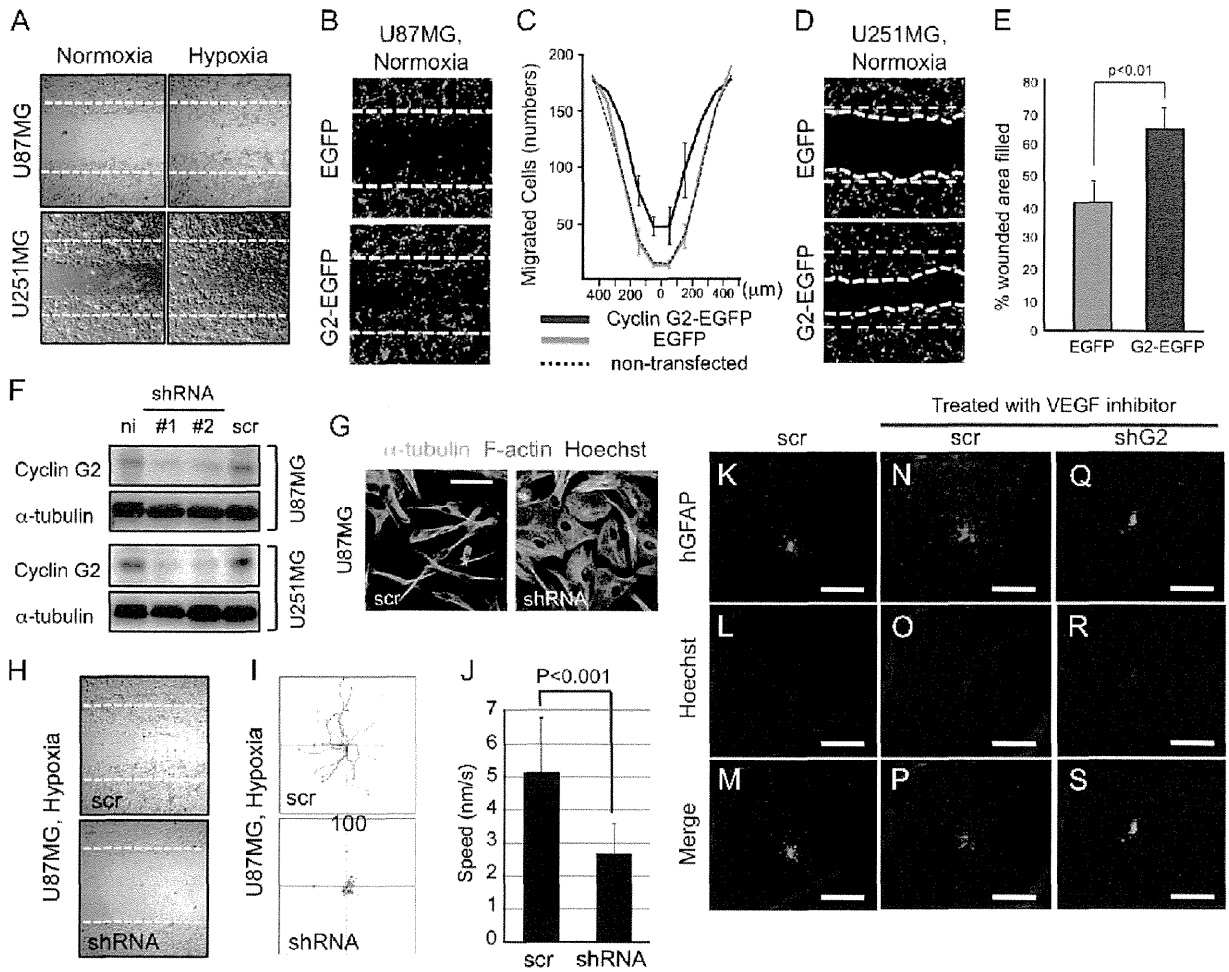

Figure 2. Cyclin G2 promotes glioblastoma cell migration and is required for the hypoxia-driven invasion of glioblastoma. (A) Hypoxia promotes the migration of glioma cells. (B–E) Wound-healing assay showing that forced expression of cyclin G2 promotes the migration even under normoxic conditions. The histograms show the number of EGFP-positive migrating cells in cyclin G2–EGFP– or EGFP-transfected U87MG cells (C) or the filled wounded area in U251MG cells (E). (F) U87MG and U251MG cells were infected with retroviral vectors encoding shRNA against human *ccng2* or scrambled shRNA. (G) A reduction in cyclin G2 expression changes the cell shape from spindle to flat in U87MG cells. (H–J) Knockdown of cyclin G2 results in reduced wound healing (H) and cellular motility (I). Motile speed is reduced by almost half (J). (K–S) Antiangiogenic treatment promotes the local invasion of glioblastoma cells in a cyclin G2–dependent manner. U251MG cells treated with shRNA against *ccng2* did not show migration induced by CBO-P11 treatment. The scale bars represent 20 μm (G) or 500 μm (K–S).

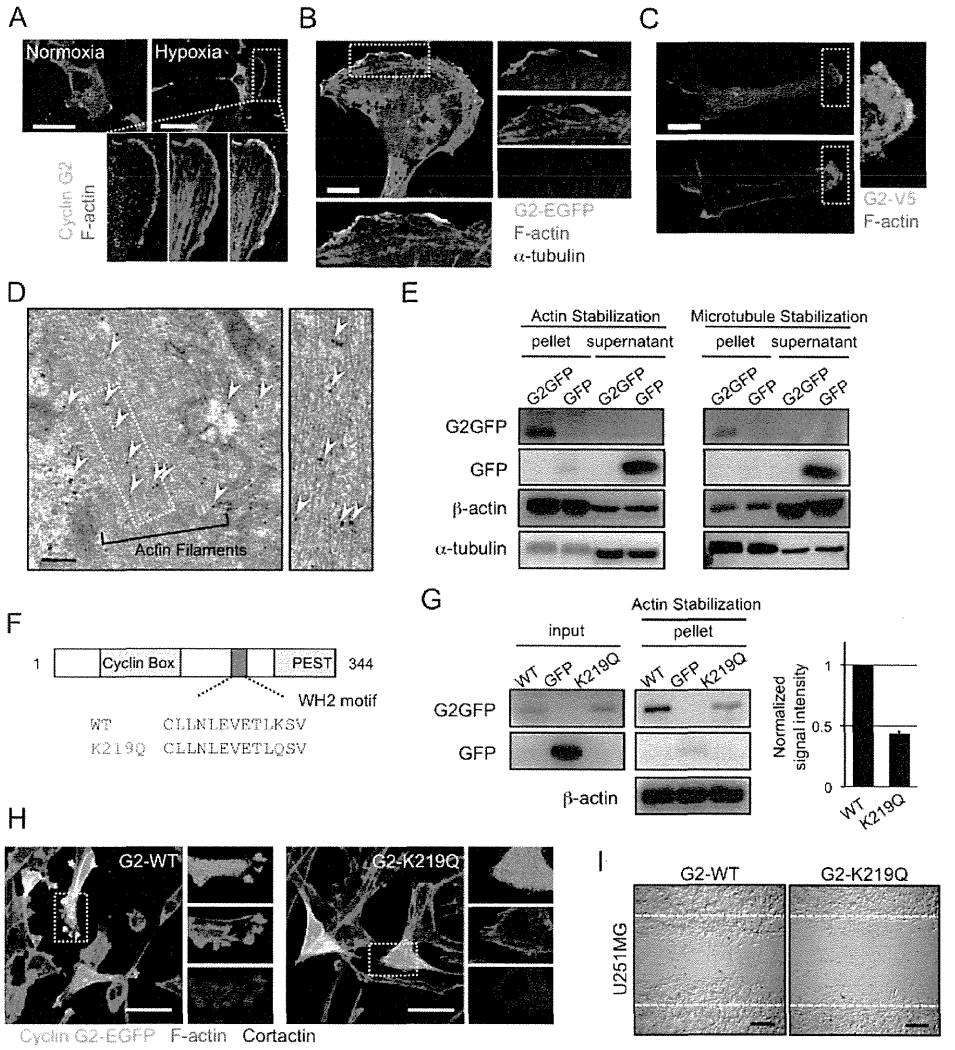

Figure 3. Cyclin G2 interacts with actin filaments, and the interaction is required for the motility of glioblastoma cells. (A) Endogenous cyclin G2 (green) localizes at the leading edge of migrating U87MG cells merging with F-actin (red). In hypoxia-stimulated U87MG cells, endogenous cyclin G2 accumulated at membrane ruffles. (B and C) Exogenously expressed cyclin G2–EGFP (B) and cyclin G2–V5 (C) also localize at the ruffles. (D) Immunoelectron microscopy of U87MG cells transfected with cyclin G2–EGFP. Arrowheads indicate the immunogold labeling of EGFP. (E) Cyclin G2 interacts with both filamentous actin and microtubules. (F) Cyclin G2 has a putative WH2 motif. (G–I) The K219Q mutant impairs the interaction with actin filaments (G), the potentiation of ruffle formation (H), and the consequent migration (I). Cortactin (blue) served as a marker of membrane ruffles (H). The scale bars represent 50 μm (A, H), 10 μm (B, C), 200 nm (D), or 200 μm (I).

invasion did not emerge (Figure 2, *Q–S*). These findings show that cyclin G2 is involved in the hypoxia-driven local invasion of glioblastoma.

Cyclin G2 Is a Cytoskeleton-Associated Protein

To examine the molecular mechanism of the cyclin G2–dependent tumor expansion, we next performed immunofluorescent analyses to detect the distribution of endogenous and exogenous cyclin G2 in glioma cells. Cyclin G2 occurred in the cytoplasm of U87MG cells in a normoxic and steady state (Figure 3*A*). However, under hypoxic conditions, the endogenous cyclin G2 accumulated at the leading edge, often referred to as membrane ruffles, merging with actin filaments (Figure 3*A*). The exogenously expressed cyclin G2–EGFP or cyclin G2–V5 also showed a peripheral distribution even under normoxic conditions (Figure 3, *B* and *C*). Immunoelectron microscopic analysis confirmed the co-localization of cyclin G2 and actin filaments (Figure 3*D*). In a previous study, cyclin G2 was shown to interact with microtubules [13]. To further understand the association between cyclin G2 and the cytoskeleton, we prepared a cytoskeletal pellet mainly containing actin filaments or microtubules (for details, see Materials and Methods section). Intriguingly, cyclin G2 was observed in the pellet under both actin-stabilizing (phalloidin and nocodazole treatment) and microtubule-stabilizing (latrunculin B and paclitaxel treatment) conditions (Figure 3*E*). On the basis of the ELM database prediction, cyclin G2 has a putative, actin-interacting WH2 motif (Figure 3*F*). To check whether cyclin G2 interacts with

actin filaments through this motif and affects actin polymerization, we prepared a K219Q mutant, which lacks the essential lysine in the WH2 motif [29]. In the actin-stabilized pellet, we observed a decreased signal of the K219Q mutant compared to wild-type cyclin G2, but total amounts of actin signals in the pellet seemed to be unchanged (Figure 3*G*). Moreover, the K219Q mutant lacks the potentiation of cyclin G2–induced ruffle formation and migration (Figure 3, *H* and *I*). These findings suggested that cyclin G2 interacted with actin filaments and affected the cytoskeletal dynamics at the leading edge of migrating cells using a certain mechanism, not promoting actin polymerization.

Cyclin G2 Promotes the Restricted Tyrosine Phosphorylation of Cortactin

We investigated the possibility that cyclin G2 might interact with cortactin and dynamin 2, actin-binding proteins and targets of oncogene src kinases [30], because they are well-defined regulators of actin dynamics and facilitators of ruffle formation, invadopodia formation, and consequent tumor invasion [31–33]. In glioblastoma cells, cyclin G2 co-localized with actin filaments and cortactin, or dynamin 2 at ruffles (Figure 4, *A* and *B*), and interacts with endogenous cortactin and dynamin 2 (Figure 4*C*). Notably, cyclin G2's reduction impaired cortactin's recruitment to the juxtamembrane and ruffle formation triggered by hypoxia (Figure 4, *D* and *E*), not by affecting cortactin expression levels (Figure 4*F*). These observations led to a hypothesis that enhanced expression of cyclin G2 owing to hypoxia or exogenous treatment influences actin dynamics and cellular motility by regulating cortactin or dynamin 2 function. In the regulation of actin dynamics in which cortactin and dynamin 2 are involved, tyrosine phosphorylation of cortactin is essential [34], and SFKs are required for the phosphorylation and consequent invasion [35]. Therefore, we investigated cortactin or dynamin 2 phosphorylation by immunoprecipitation and immunoblot analysis. In hypoxia-treated U87MG cells, cortactin, but not dynamin 2, was tyrosine-phosphorylated in an SFK-dependent manner (Figure 4*G*). This phosphorylation was also observed in hypoxic regions, typically pseudopalisades in glioblastoma specimens (Figure 4*H*), and seemed to be related to the abundance of cyclin G2 (Figure 4*I*). Surprisingly, even under normoxic conditions, the exogenously expressed cyclin G2 (tagged with EGFP or V5) also induced cortactin phosphorylation in an SFK-dependent manner (Figure 4, *J* and *K*). Elevated levels of cyclin G2 did not increase the total amount of tyrosine-phosphorylated protein (Figure W5*A*). These results show that abundant cyclin G2 induces the restricted tyrosine phosphorylation of cortactin. This could be explained by the fact that cyclin G2 was required for the localization of cortactin to the juxtamembrane, where SFKs phosphorylated cortactin. Ectopic cyclin G2 enhances the peripheral signal of phosphotyrosine in an SFK-dependent manner (Figure W5*B*). Furthermore, the increased motility by exogenous cyclin G2 as observed in Figure 2, *B* to *E*, was blocked by dasatinib but not erlotinib (Figure 4*L*). Although cyclin G2 binds to an active PP2A complex, the tyrosine phosphorylation of cortactin induced by abundant cyclin G2 was not influenced by okadaic acid (PP2A inhibitor) or D-*erythro*-S (PP2A activator) treatment (Figure 4*M*).

Cyclin G2 Is an SH3 Domain–Containing Protein that Provides a Functional Connection of Src, Cortactin, and Actin Cytoskeleton at the Ruffles

In primary glioblastoma, SFK expression was enhanced in the glioma cells that also expressed cyclin G2 abundantly (Figure 5*A*). In U87MG cells, hypoxic conditions enhanced, whereas ectopic cyclin G2 did not induce, the expression of fyn and src, which are effectors of oncogenic epidermal growth factor receptor signals in glioblastoma [36] (Figures 5*B* and W5*C*). These observations support our findings above that cyclin G2 promotes cortactin phosphorylation and consequent migration in concert with SFKs, and it may be appropriate to presume that the hypoxia-induced, excessive expression of cyclin G2 and SFKs synergistically potentiates the hypoxia-driven local invasion through the restricted tyrosine phosphorylation of cortactin.

Next, we examined the biochemical interaction between cyclin G2, cortactin, and SFKs. These proteins were co-immunoprecipitated (Figure 5*C*). According to the ELM-based prediction that cyclin G2 has a putative SH2 domain–binding motif and a noncanonical SH3 domain–binding motif (Figure 5*D*), we expected the N terminus of cyclin G2 to be important for cyclin G2–SFK interactions and the C terminus for cortactin phosphorylation. SH2 domain–containing proteins such as SFKs target phosphotyrosine-containing peptides in a sequence-specific manner [37]. As expected, we found that cyclin G2 was tyrosine-phosphorylated in an SFK-dependent manner (Figure 5*E*) and deletion of the N terminus in cyclin G2 (ΔN-G2) impaired cyclin G2–Src interaction (Figure 5*F*). A past study showed that a noncanonical SH3 domain–binding motif (PxxPxxP) was important for interaction with an SH3 domain–containing protein, cortactin [38]. The G2-P291A mutant ($G2^{P291A}$, which has a critical mutation in a noncanonical SH3 domain–binding motif) showed no interaction with cortactin and the consequent induction of tyrosine phosphorylation of cortactin and migration (Figures 5, *G* and *H*, and W5*D*). The $G2^{P291A}$ mutant did not cause ruffle formation and the recruitment of cortactin to the juxtamembrane in U87MG cells (Figure 5, *I–N*). Furthermore, to evaluate the effect of dasatinib on the tumor expansion induced by antiangiogenic treatment, we intracranially implanted U251MG cells and treated them with CBO-P11 alone or CBO-P11 plus dasatinib. As expected, dasatinib efficiently inhibited the expansion of glioma cells induced by CBO-P11 treatment (Figure 5, *O–T*). Combined with the results in Figure 2, *K* to *S*, these findings showed that the cyclin G2–SFKs–cortactin axis was required for the local invasion induced by hypoxia or antiangiogenic treatment *in vitro* and *in vivo* and the inhibition of SFKs by dasatinib attenuated it and that cyclin G2 acted upstream of SFK-cortactin.

Discussion

In summary, we demonstrated that cyclin G2 played pivotal roles in the regulation of actin dynamics in the hypoxia-driven local invasion of glioblastoma cells (Figure 5*U*). Severe hypoxia enhanced the expression of cyclin G2 and SFKs and the consequent formation of ruffles and cell migration by modulating the tyrosine phosphorylation of cortactin. Cyclin G2 orchestrates the recruitment to the juxtamembrane and SFK-dependent tyrosine phosphorylation of cortactin and thereby actin dynamics. We revealed that the SH2 or SH3 domain–binding motif and WH2 motif in cyclin G2 were important for this mechanism. Furthermore, we also found that cyclin G2 was a target of SFKs and phospho-cyclin G2 seemed to prefer the actin interaction. These findings provide the first evidence that cyclin G2 is a key regulator in the hypoxia-driven migration of glioblastoma cells. We are now investigating the relationship between cyclin G2 and other regulators of actin dynamics such as cdc42, rac1,

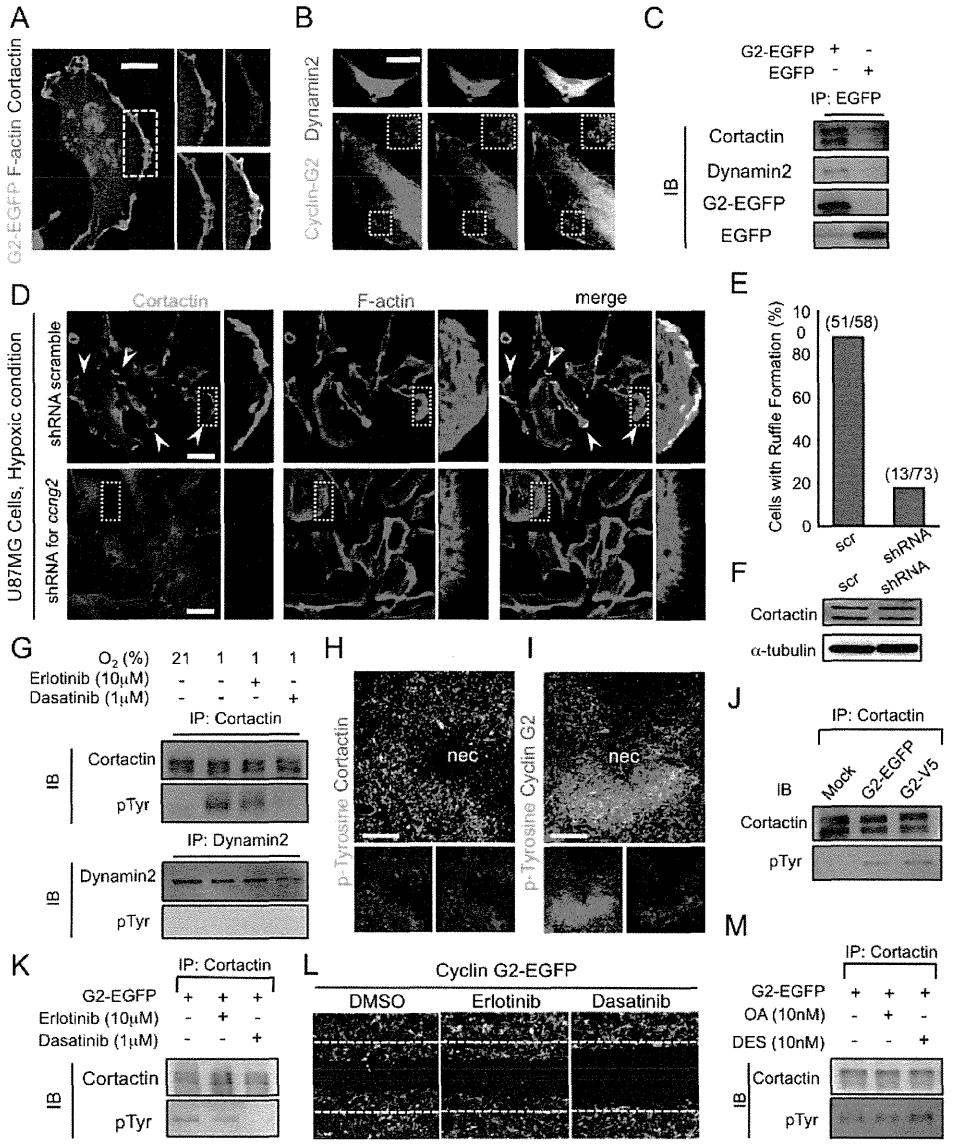

Figure 4. Cyclin G2 orchestrates cortactin tyrosine phosphorylation and the consequent migration of glioblastoma cells in concert with SFKs. (A and B) Cyclin G2 (green) co-localizes with F-actin (red) and cortactin (blue) (A), or dynamin 2 (B) at membrane ruffles. (C) Immunoprecipitation analysis shows that cyclin G2 interacts with endogenous cortactin and dynamin 2. (D–F) Cyclin G2 is required for the ruffle formation in response to hypoxia and the recruitment of cortactin to the juxtamembrane in glioblastoma cells (D). U87MG cells transfected with shRNA for human *ccng2* (lower panels) show fewer membrane ruffles than control cells (upper panels) in hypoxic conditions (E). Knockdown of cyclin G2 does not alter the expression level of cortactin (F). (G) Hypoxia induces tyrosine phosphorylation of cortactin, but not dynamin 2, in an SFK-dependent manner. (H and I) Phosphotyrosine signals are abundant near necrotic regions, merging with cortactin (H) and cyclin G2 (I). (J) Forced expression of cyclin G2 enhances the tyrosine phosphorylation of cortactin even under normoxic conditions. U87MG cells were transfected with cyclin G2–EGFP or cyclin G2–V5. (K) The tyrosine phosphorylation of cortactin induced by cyclin G2 is inhibited by dasatinib but not erlotinib. (L) Cyclin G2–enhanced wound healing is inhibited by dasatinib but not erlotinib. (M) PP2A activity seems to have no impact on the tyrosine phosphorylation. The scale bars represent 10 μm (A), 20 μm (B, D), or 200 μm (H, I).

and rhoA and the possibility that cyclin G2 affects signal transduction in which tyrosine phosphorylation is essential.

Concerning the therapeutic strategy for glioblastoma expansion, inhibiting the hypoxia-driven local invasion is imperative. According to our findings, decreasing the level of cyclin G2 is sufficient to inhibit the invasion (Figure 2, *K–S*). However, the reduction results in excessive proliferation because cyclin G2 acts as a negative regulator of the cell cycle (Figure W3, *B* and *C*). In the mechanism of the local invasion in which cyclin G2–SFKs–cortactin axis is involved, inhibiting SFKs is effective both *in vitro* and *in vivo*, in various cells including glioma-initiating cells (Figures 4, 5, and W6). Recent studies showing that SFKs such as fyn and src are ideal targets for glioblastoma expansion [35,36] support our observations.

Exactly why cyclin G2 determines cell behavior according to tumor origins remains unclear. As mentioned, cyclin G2 expression is enhanced by Nodal, a member of the transforming growth factor β superfamily. Interestingly, Nodal was recently identified as a facilitator of glioblastoma expansion [27], whereas it inhibits carcinoma expansion. Moreover, in breast carcinoma, p63, a master regulator of epithelial but not glial cell fate, is a key factor in the expression of cyclin G2, which is controlled by transforming growth factor β–Smad2 signaling [15]. Further studies are needed, but the different effects of cyclin G2 on tumor expansion may be because of signaling pathways that control carcinoma and glioma behavior.

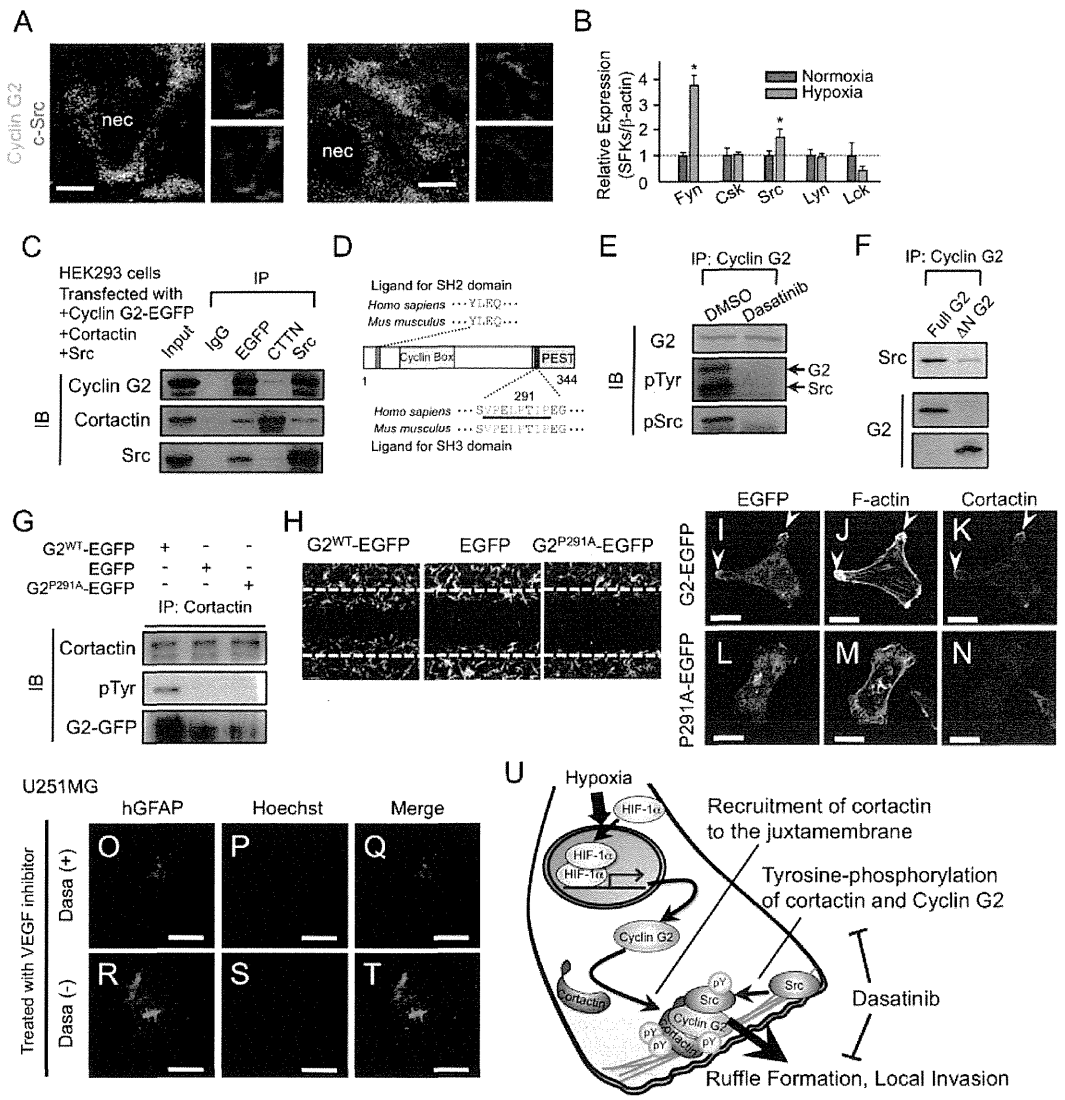

Figure 5. Molecular mechanism of the cyclin G2–driven tyrosine phosphorylation of cortactin and consequent invasion. (A) Immunofluorescent analysis showing that c-Src is abundantly expressed in pseudopalisades and most signals overlap with signals for cyclin G2. (B) Hypoxia significantly promotes the transcription of SFKs, Fyn, and Src in U87MG cells. (C) Cyclin G2, cortactin, and SFKs are co-immunoprecipitated. (D) Schematic diagram of the cyclin G2 protein. Cyclin G2 has a putative SH2 domain–binding motif at the N terminus and a noncanonical SH3 domain–binding motif (bar; 287-294) at the C terminus. Green letters indicate aliphatic amino acids (valine, leucine, and isoleucine), and red letters indicate proline. (E) Immunoprecipitation and immunodetections in HEK293 cells transfected with cyclin G2–EGFP and Src. Cyclin G2 is tyrosine-phosphorylated in an SFK-dependent manner. (F) Deletion of the N terminus (ΔN-G2) of cyclin G2 impairs the interaction with Src. (G and H) A single amino acid mutation (P291A) in the SH3 domain–binding motif of cyclin G2 ($G2^{P291A}$) impaired the induction of cortactin tyrosine phosphorylation (G) and consequent cell migration (H). (I–N) The P291A mutant impairs recruitment of cortactin to juxtamembrane. (O–T) Dasatinib inhibited the GBM expansion enhanced by anti–vascular endothelial growth factor treatment. (U) A model describing the role of cyclin G2 in the hypoxia-driven local invasion of glioblastoma cells. Cyclin G2 recruits cortactin to the leading edge of migrating glioma cells and promotes the consequent tyrosine phosphorylation of cortactin, which is essential for ruffle formation and tumor invasion. The scale bars represent 200 μm (A, O–T); "nec" indicates the necrotic foci in GBM specimens.